






Geothermobarometry and geochemical modeling of Archean charnockites from Carajás Province, Amazonian craton, Brazil

Bhrenno Marangoanha^{1*} , Davis Carvalho de Oliveira¹ , Cláudio Nery Lamarão¹ , Gisele Tavares Marques¹ , Luciano Ribeiro da Silva¹ 

Abstract

Orthopyroxene-bearing tonalites/trondhjemites with scarce quartz diorites comprise the Café enderbite that crops out in three Neoproterozoic plutons in the central portion of the Canaã dos Carajás domain, Carajás Province, northern Brazil. Intrinsic parameters based on the mineral chemistry of plagioclase, biotite, amphibole, and pyroxene constrain crystallization conditions to 1150–850°C and 750–600 MPa, moderate water content in the melt (4.8–5.6 wt.%) and relatively oxidizing conditions, between the fayalite–magnetite–quartz (FMQ) and nickel–nickel oxide (NNO) + 1.7 buffers. Geochemical modeling indicates that the Café enderbite evolved via at least two fractional crystallization stages – quartz diorite to orthopyroxene tonalite and orthopyroxene tonalite to orthopyroxene trondhjemite – with high crystal content (45–60%, or even higher). This high crystal content during fractional crystallization was the key factor to the preservation of orthopyroxene in the magmatic system as it left only a relatively small proportion of melt to react with early-formed orthopyroxene.

KEYWORDS: charnockite; crystallization conditions; geochemical modeling; Café Enderbite; Carajás Province.

INTRODUCTION

Although the term ‘charnockite’ was first mentioned more than one century ago by Holland (1900), its use remains confusing. Over decades, many authors have employed this term to classify both magmatic and metamorphic rocks that contain orthopyroxene (or rarely fayalite; Pichamuthu 1969, Newton 1992). According to Janardhan *et al.* (1982), Frost *et al.* (2000), and Grantham *et al.* (2012), the central reason for employing the term charnockite is that the stabilization of orthopyroxene essentially requires specific conditions, such as low water activity (a_{H_2O}) and high temperature, pressure and CO_2 , which represent deep crustal levels.

Charnockites (admitting magmatic and metamorphic origins) are typically found in Precambrian high-grade metamorphic terranes and are an important component of the middle and lower continental crust (Holland 1900, Brown 1994, 2004, 2007, Kriegsman 2001). The igneous rocks are

extremely valuable petrologically because they contain orthopyroxene and have relatively unvaried assemblages, which permits the calculation of their crystallization parameters (e.g., temperature, pressure, oxygen fugacity, and water content) with a much greater precision than most other pyroxene-free granitic rocks (Frost and Frost 2008).

Carajás Province (Amazonian craton, Brazil) records significant occurrences of charnockitic series rocks, in which orthopyroxene has been attributed to a magmatic origin (Santos *et al.* 2013, Marangoanha *et al.* 2019a, Félix *et al.* 2020). These rocks comprise a wide compositional range, varying from granodiorites to tonalites and trondhjemites, with associated quartz diorites and gabbros, and their investigation has produced important understanding concerning the Neoproterozoic evolution in this portion of the crust.

In the central portion of the Canaã dos Carajás domain (Carajás Province), the Neoproterozoic Café enderbite crops out as three lenticular plutons (~5 km long) composed dominantly of orthopyroxene-bearing tonalite and trondhjemite, with subordinate quartz diorite. In this article, we report the mineralogical characteristics of this enderbite and discuss its intrinsic crystallization parameters. Geochemical modeling techniques were also employed to quantitatively evaluate the petrogenetic processes that account for the evolution of these charnockites. We compare the results of this study with those for similar occurrences worldwide, particularly with Archean–Proterozoic associations, in an attempt to discuss and constrain the petrogenesis and crystallization parameters that play a role in this specific type of magmatism.

Supplementary data

Supplementary data associated with this article can be found in the online version: <http://sfbjg.siteoficial.ws/Sf/2022/4889202220210092.pdf>.

¹Grupo de Pesquisa Petrologia de Granitoides, Instituto de Geociências, Universidade Federal do Pará – Belém (Pará), Brazil. E-mails: bhrenno@ufpa.br, davis@ufpa.br, lamarao@ufpa.br, giseletm@ufpa.br, lucianor@ufpa.br

*Corresponding author.



GEOLOGICAL SETTING

Carajás Province represents the oldest Archean nucleus in the Amazonian craton, northern Brazil (Tassinari and Macambira 2004; Fig. 1A), and comprises three lithotectonic domains: Rio Maria, Sapucaia, and Canaã dos Carajás; the last domain is considered the basement of the Carajás basin (Dall'Agnol *et al.* 2013; Fig. 1B). The Rio Maria domain (2.98–2.86 Ga) is located in the southern part of Carajás Province and consists of greenstone belts, tonalite-trondhjemite-granodiorite (TTG) rocks, sanukitoids, and leucogranites-leucogranodiorites (Althoff *et al.* 2000, Souza *et al.* 2001, Leite *et al.* 2004, Dall'Agnol *et al.* 2006, Oliveira *et al.* 2009, Almeida *et al.* 2010,

2011, Guimarães *et al.* 2010). Immediately to the north, the Sapucaia domain presents practically the same lithology as the Rio Maria domain, except that the former records ~2.74 Ga granitic events represented by deformed Neoproterozoic A-type granitoids (Dall'Agnol *et al.* 2013, 2017, Silva *et al.* 2020).

In contrast to the first two domains above, the Canaã dos Carajás domain displays a more heterogeneous lithology (Feio *et al.* 2012, Dall'Agnol *et al.* 2013) and represents a high-grade granulitic terrane with complex geologic evolution (Pidgeon *et al.* 2000, Marangoanha *et al.* 2019a, 2020, Silva *et al.* 2021). Mesoarchean units (3.06–2.83 Ga) are composed of granulites, orthogneisses, migmatites, tonalites, trondhjemites, and

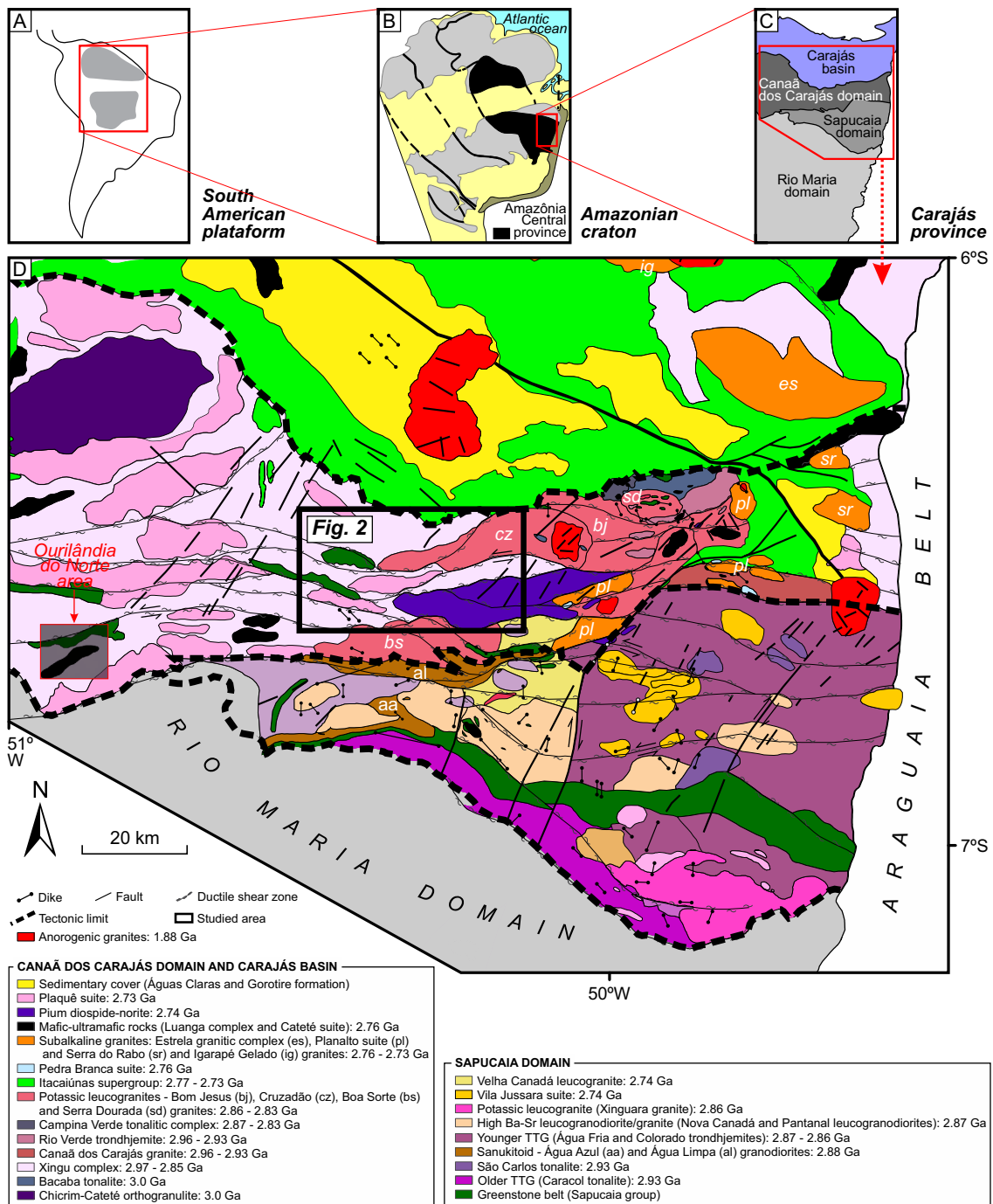


Figure 1. (A) South American platform. (B) Amazonian craton. (C) Geological map of Carajás Province showing the boundaries between the Rio Maria, Sapucaia, and Canaã dos Carajás domains, in addition to the Carajás basin (Dall'Agnol *et al.* 2013). (D) Detailed geological sketch map of the Canaã dos Carajás domain, modified after Gabriel and Oliveira (2014). The black-colored rectangle in (D) corresponds to the area of Fig. 2.

granites (Machado *et al.* 1991, Avelar *et al.* 1999, Pidgeon *et al.* 2000, Moreto *et al.* 2011, Feio *et al.* 2013, Melo *et al.* 2014, Rodrigues *et al.* 2014, Marangoanha *et al.* 2019a, Silva *et al.* 2021). The Neoproterozoic units (2.77–2.70 Ga) are represented by granitic and mafic-ultramafic rocks, charnockites-enderbites, greenstone belts, and sedimentary rocks (Nogueira *et al.* 1995, Vasquez *et al.* 2008, Dall'Agnol *et al.* 2013, Marangoanha *et al.* 2019a, 2019b, 2020; Fig. 1C). At 1.88–1.86 Ga, the entire Carajás Province was affected by the emplacement of anorogenic granites and associated dikes (Dall'Agnol *et al.* 2005, Teixeira *et al.* 2019 and references therein).

CHARNOCKITIC MAGMATISM OF CARAJÁS PROVINCE

The first records of rocks from the charnockitic series (admitting its igneous origin) have been documented recently in Carajás Province, when the Geological Survey of Brazil (CPRM) redefined the 'granulitic' Pium complex unit as the 'igneous' Pium diopside-norite (Vasquez *et al.* 2008), which was later corroborated by Santos *et al.* (2013), who obtained Neoproterozoic crystallization ages of 2.74–2.73 Ga for gabbro-norite, orthopyroxene-bearing quartz gabbro, diorite, and tonalite related to this unit. Marangoanha *et al.* (2019a) identified orthopyroxene-bearing tonalite, trondhjemite, and scarce quartz diorite, formally named the Café enderbite, forming three E–W-trending lenticular plutons (up to ~5 km long) associated spatially with the Pium diopside-norite dated at 2.75–2.73 Ga. Through geochemical modeling, these authors attributed generation of the less evolved melt (quartz diorite) from this enderbite assemblage to partial melting of a mafic granulitic source. Additionally, Marangoanha *et al.* (2019a, 2020) excluded any cogenetic link between the Café enderbite and

the Pium diopside-norite through isotope data (Café enderbite: $\epsilon\text{Hf}_{(2.74\text{ Ga})}$ between –4.8 and –1.9; Pium diopside-norite: $\epsilon\text{Nd}_{(2.74\text{ Ga})}$ between –0.5 and +0.7). In the Ourilândia do Norte area, Félix *et al.* (2020) attributed a Neoproterozoic pluton composed of orthopyroxene-bearing granodiorite and monzogranite to an origin related to fractional crystallization of gabbro-norite magma.

In addition to the aforementioned occurrences, two Neoproterozoic units should be mentioned: the Vila Jussara and Vila União suites. The Vila Jussara suite consists of pyroxene-free and amphibole-bearing monzogranites and granodiorites. This led Dall'Agnol *et al.* (2017) to interpret these rocks as 'hydrated granites associated with charnockites' representing the transition from anhydrous to hydrous granitoids according to the proposal of Frost and Frost (2008). The Vila União suite is a hybrid series composed of quartz diorite, tonalite, granodiorite, and syeno-monzogranite formed by mixing between crustal anatexis and mantle-derived magmas, in which the orthopyroxene present in these hybrid granitoids corresponds to xenocrysts from the mafic endmember (Marangoanha *et al.* 2020).

GENERAL ASPECTS OF THE CAFÉ ENDERBITE

The Café enderbite plutons crop out in the Ouro Verde area and are composed of orthopyroxene-bearing sodic granitoids (Marangoanha *et al.* 2019a). These plutons crosscut Mesoproterozoic units represented by the Ouro Verde granulite and Cruzadão granite and are spatially associated with the coeval Pium diopside-norite and hybrid granitoids from the Vila União suite (cf. Fig. 2; Marangoanha *et al.* 2020). These rocks are inserted in the tectonic context of the regional-scale Mesoproterozoic (ca. 2.8 Ga)

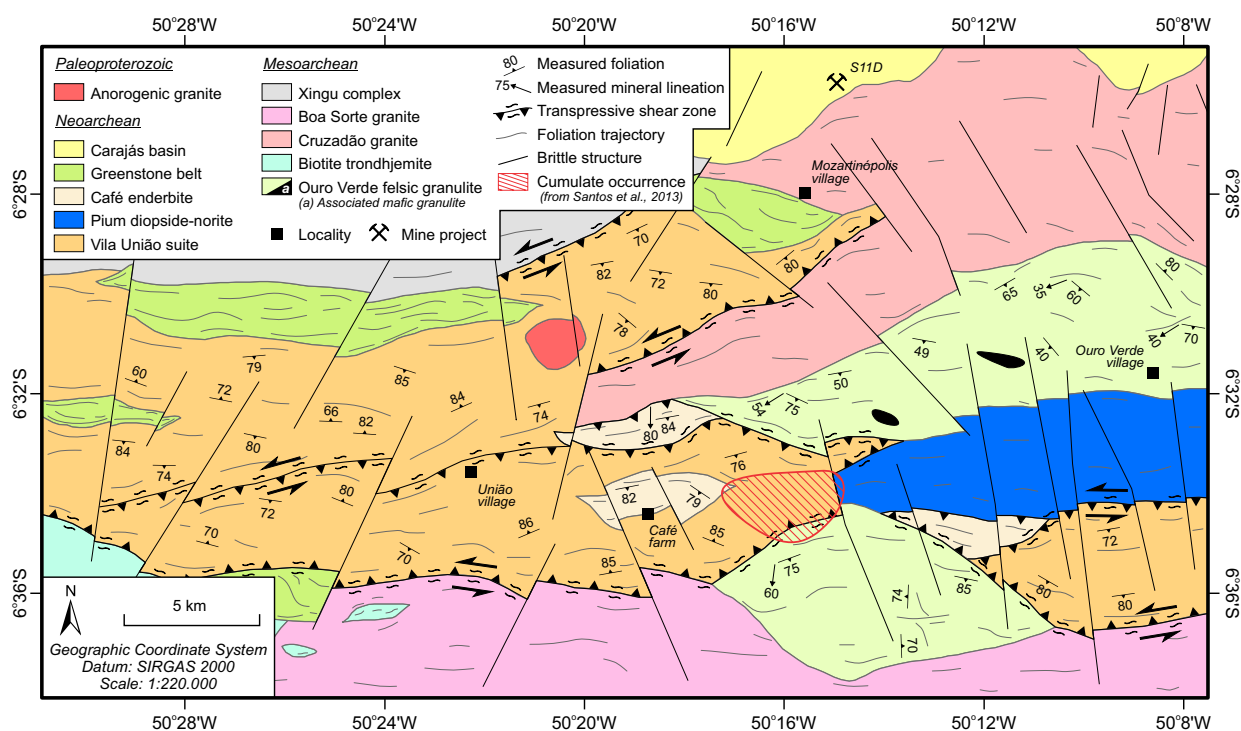


Figure 2. Geological map of the study area.

E–W-trending Itacaiúnas shear zone (Holdsworth and Pinheiro 2000). According to Marangoanha *et al.* (2019a), the Café enderbite plutons may have grown through amalgamation of sequentially intruded sheets or relatively small magmatic pulses emplaced along this ancient Mesoproterozoic shear structure, which was reactivated in the Neoproterozoic, resulting in elongated bodies parallel to the major E–W-trending compression.

Mesoscopically, the studied granitoids show a homogeneous appearance; they are gray white in color, equigranular, medium grained, and mostly leucocratic (Fig. 3A), with minor mesocratic

occurrences (Fig. 3B). The general petrographic aspects of the Café enderbite have been discussed by Marangoanha *et al.* (2019a). These authors considered that although mylonitization is present in these rocks, they still exhibit significant original magmatic textures; this also implies that their original mineral assemblage remains unchanged and thereby allows their magmatic conditions to be estimated through the application of specific geothermobarometers. These granitoids have plagioclase, quartz, biotite, amphibole, clinopyroxene, orthopyroxene, and opaque minerals as the main minerals (Figs. 3C–3F; Tab. 1), and when

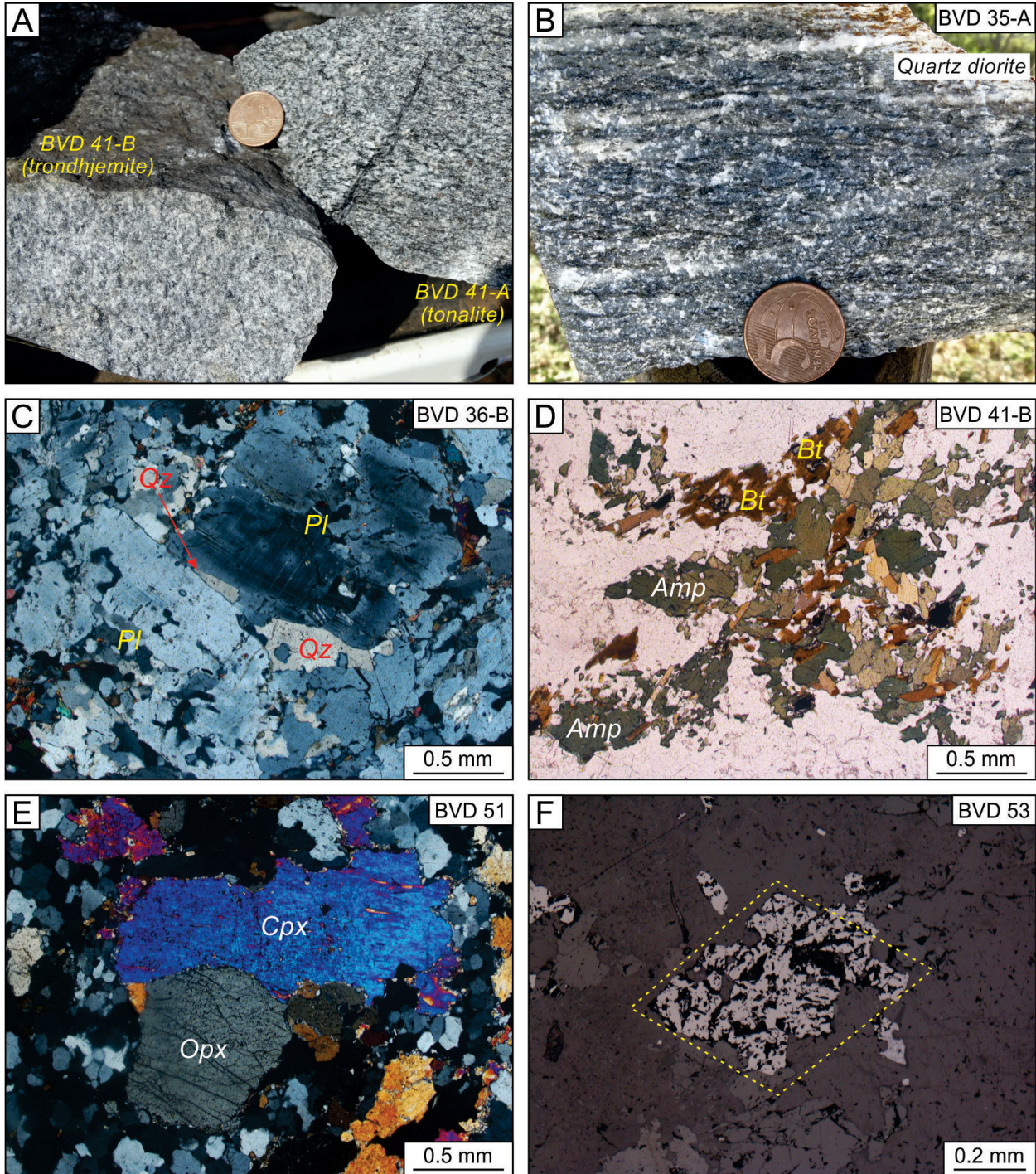


Figure 3. Mesoscopic and microscopic aspects showing preserved igneous textures of the rocks from the Café enderbite. (A) Medium-grained granitoids with tonalitic and trondhjemitic compositions, equigranular and gray-white in color. (B) Medium-grained quartz diorite showing homogeneous appearance. (C) Subhedral plagioclase (Pl) grains with interstitial quartz (Qz). (D) Fine-grained amphibole (Amp) associated with biotite (Bt). (E) Common occurrence of orthopyroxene and clinopyroxene (Opx and Cpx, respectively). (F) Subhedral primary magnetite. Photomicrographs (C) and (E) were taken under crossed nicols, (D) under parallel nicols, and (F) under reflected light.

plotted in the quartz-alkali feldspar-plagioclase (QAP) diagram of Le Maitre *et al.* (2002), they lie predominantly in the tonalitic/trondhjemitic field, with subordinate quartz diorite (Fig. 4). The International Union of Geological Sciences (IUGS) classification for orthopyroxene-bearing granitoids (Streckeisen 1974) identifies these rocks as enderbites.

Geochronological and isotopic data obtained by Marangoanha *et al.* (2019a) reveal crystallization ages of 2.75–2.73 Ga for these granitoids, with low $\epsilon\text{Hf}(t)$ values (between –4.8 and –1.9 epsilon units) and Hf-T_{DM2} ages of 3.46–3.29 Ga, implying relatively long crustal residence times for these rocks (~700–500 Myr).

Table 1. Summary of modal compositions of the Café enderbite*.

Variety	Quartz diorite	Tonalite	Trondhjemitic
Minerals (vol.%)			
Quartz	7-9	21-30	34-38
Plagioclase	51-67	51-64	54-62
Alkali feldspar	-	<i>p</i>	-
Biotite	-	0-15	0-5
Amphibole	4-6	4-15	0-4
Clinopyroxene	10-22	0-3	<i>p</i>
Orthopyroxene	5-12	1-3	<i>p</i>
Opaque minerals	1-5	0-4	1-2
Titanite	-	<i>p</i>	<i>p</i>
Epidote	<i>p</i>	<i>p</i>	-
Allanite	-	<i>p</i>	-
Zircon	-	<i>p</i>	<i>p</i>
Chlorite	-	<i>p</i>	0-2

p: present but < 1%; -: not determined; *the complete data are presented in Marangoanha *et al.* (2019a).

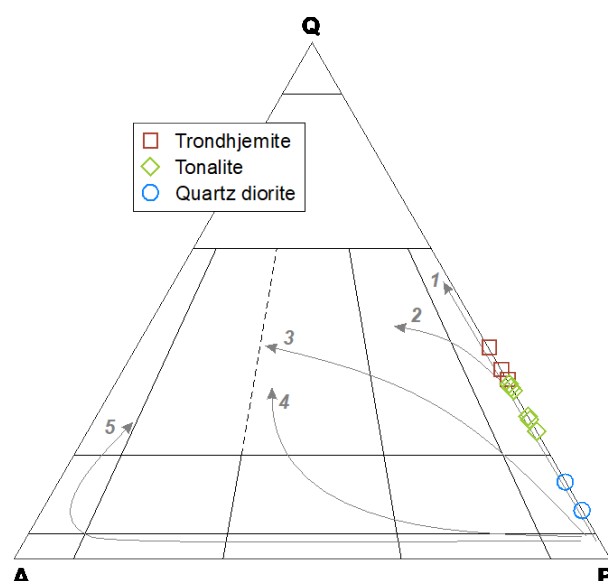


Figure 4. The QAP plot for the granitoids from the Café enderbite (Le Maitre *et al.* 2002). Granitic series and their evolutionary trends are from Lameyre and Bowden (1982) and Bowden *et al.* (1984): 1 (tholeiitic), 2 (calc-alkaline tonalitic or trondhjemitic), 3 (calc-alkaline granodioritic), 4 (subalkaline monzonitic or shoshonitic), and 5 (alkaline and peralkaline).

MINERAL CHEMISTRY

Methodology

The major element compositions of plagioclase, biotite, amphibole, and pyroxene, obtained from four thin sections, were measured by wavelength dispersive electron probe microanalysis (EPMA) in the Laboratório de Microanálises at the Geosciences Institute of the Universidade Federal do Pará (UFPA), Brazil. EPMA was performed with a JEOL JXA-8230 instrument with five wavelength dispersive spectrometers, a 15-kV acceleration voltage, a beam current of 20 nA, and an acquisition time of 20 s. The crystals used for the analyses were TAP for Na, Si, Al, and Mg; PETJ for K, Ca, Cr, and Sr; LIF for Ni, Fe, Ti, Mn, and Ba; PETH for V and Cl; and LDE1 for F. The standards used for instrument calibration were microcline (Si, Al, and K), albite (Na), andradite (Fe and Ca), pyrophanite (Ti and Mn), vanadinite (Cl and V), forsterite (Mg), and topaz (F).

Mineral compositions

Plagioclase

The EPMA results presented in Suppl. Tab. A and plotted in the Ab-An-Or diagram by Deer *et al.* (1992; Fig. 5A) show that plagioclase grains from the Café enderbite fall in the oligoclase and andesine fields. The plagioclase grains from the trondhjemitic variety are classified as oligoclase and displays extremely narrow compositional ranges, varying from An_{15} to An_{18} . On the other hand, plagioclase grains from the tonalitic variety present variable and more calcic compositions, ranging from oligoclase to andesine (An_{20} to An_{40}). Plagioclase in the quartz dioritic rocks presents a high degree of saussurization and does not yield reliable results.

Biotite

The chemical formulae of biotite were calculated based on 22 atoms of oxygen by using the MICA⁺ software developed by Yavuz (2003), and the results are listed in Suppl. Tab. B. This mineral is absent in the quartz dioritic variety. Biotite in the Café enderbite is enriched in MgO, with 10.86–13.38 wt.% in the trondhjemitic (number of analyses: $n = 13$) and 11.97–13.18 wt.% in the tonalites ($n = 16$). They display narrow Fe/(Fe + Mg) ratios, varying only slightly from 0.42 to 0.47 in the tonalites and 0.46 to 0.52 in the trondhjemitic, and show little variation in tetrahedral aluminum, from 2.24 to 2.31 and 2.29 to 2.34 atoms per formula unit (apfu), respectively, as shown in Fig. 5B. When referred to the $\text{Mg}-(\text{Al}^{\text{VI}} + \text{Fe}^{3+} + \text{Ti})-(\text{Fe}^{2+} + \text{Mn})$ ternary diagram of Foster (1960; Fig. 5C), biotite compositions from the analyzed rocks are clearly discriminated as magnesian biotite. All biotite lies in the primary biotite field of the $(10^*\text{TiO}_2)-(FeO + MnO)-MgO$ diagram (Fig. 5D; Nachit *et al.* 2005), suggesting that their chemical compositions were not influenced by late events and that they crystallized directly from magma.

Amphibole

The chemical compositions of the amphibole from Café enderbite are provided in Suppl. Tab. C and plotted in the

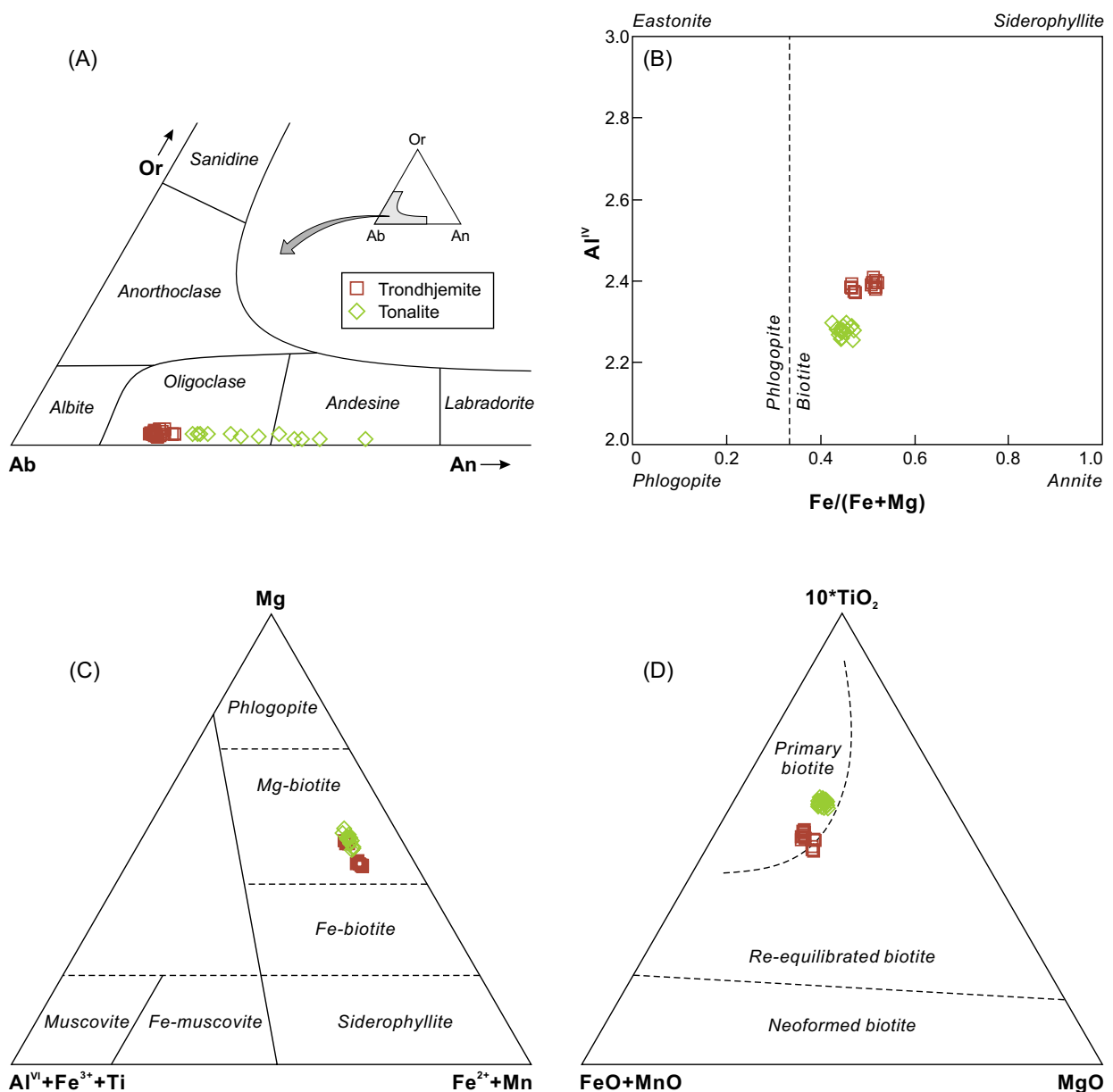


Figure 5. (A) Ab–An–Or ternary diagram showing the plagioclase compositions from the Café enderbite (after Deer *et al.* 1992). Compositional classifications of biotite after (B) Deer *et al.* (1986) and (C) Foster (1960). (D) Biotite compositions in the (10^*TiO_2) – $(FeO+MnO)$ – MgO ternary diagram (wt.%), with fields for primary (magmatic), re-equilibrated and neoformed biotite after Nachit *et al.* (2005).

$Mg/(Mg + Fe^{2+})$ versus Si diagrams by Leake *et al.* (1997). Overall, they are nearly homogeneous, and no compositional variation between crystal core and rim is detected. The amphibole from the quartz diorites have a very narrow compositional range, exhibiting X_{Mg} values between 0.42 and 0.47 and Si between 6.19 and 6.29 apfu ($n = 12$), in addition to $Fe^{3+} > Al^{VI}$, and are classified as hastingsite (Figs. 6A and 6B). The tonalitic variety has two samples analyzed: amphiboles in sample BVD 53 are similar to those in the quartz dioritic variety ($X_{Mg} = 0.36$ – 0.41 ; Si = 6.15–6.45 apfu; $Fe^{3+} > Al^{VI}$) and are also classified as hastingsite ($n = 24$; cf. Figs. 6A and 6B); amphiboles in sample BVD 36-B present higher X_{Mg} (0.63–0.75) and Si values (6.85–7.19 apfu) and are classified as Mg-hornblende ($n = 14$; Fig. 6C). Most amphiboles from trondhjemites are classified as hastingsite and ferropargasite in the same proportion ($n = 15$; cf. Figs. 6A and 6B), whereas scarce edenite is found as well ($n = 2$; cf. Fig. 6A).

Pyroxene

Pyroxene analyses from the Café enderbite are given in Suppl. Tab. D. Clinopyroxene and orthopyroxene are common in all varieties with the compositional range En_{35-50} – Fs_{14-50} – Wo_{1-48} (Fig. 7A). According to the enstatite–wollastonite–ferrosilite diagram of Morimoto *et al.* (1988), the clinopyroxenes are classified exclusively as diopside ($n = 33$; cf. Fig. 7A). Orthopyroxenes present extremely low compositional variations in terms of Fe and Mg ($X_{Mg} = Mg/(Fe^{2+} + Mg) = 0.495$ – 0.504 ; $n = 12$), and most of them are slightly richer in the ferrosilite molecule than in the enstatite molecule and are classified as ferrosilite, whereas scarce enstatite occurs as well (cf. Fig. 7A). Orthopyroxene Al content is extremely low, between 0.007 and 0.014 apfu ($X_{Al} = Al/2 = 0.004$ – 0.007). When plotted on the X_{Al} versus X_{Mg} diagram of Rajesh *et al.* (2011), which discriminates magmatic and metamorphic orthopyroxenes in charnockitic assemblages, all orthopyroxenes present a clear magmatic origin (Fig. 7B).

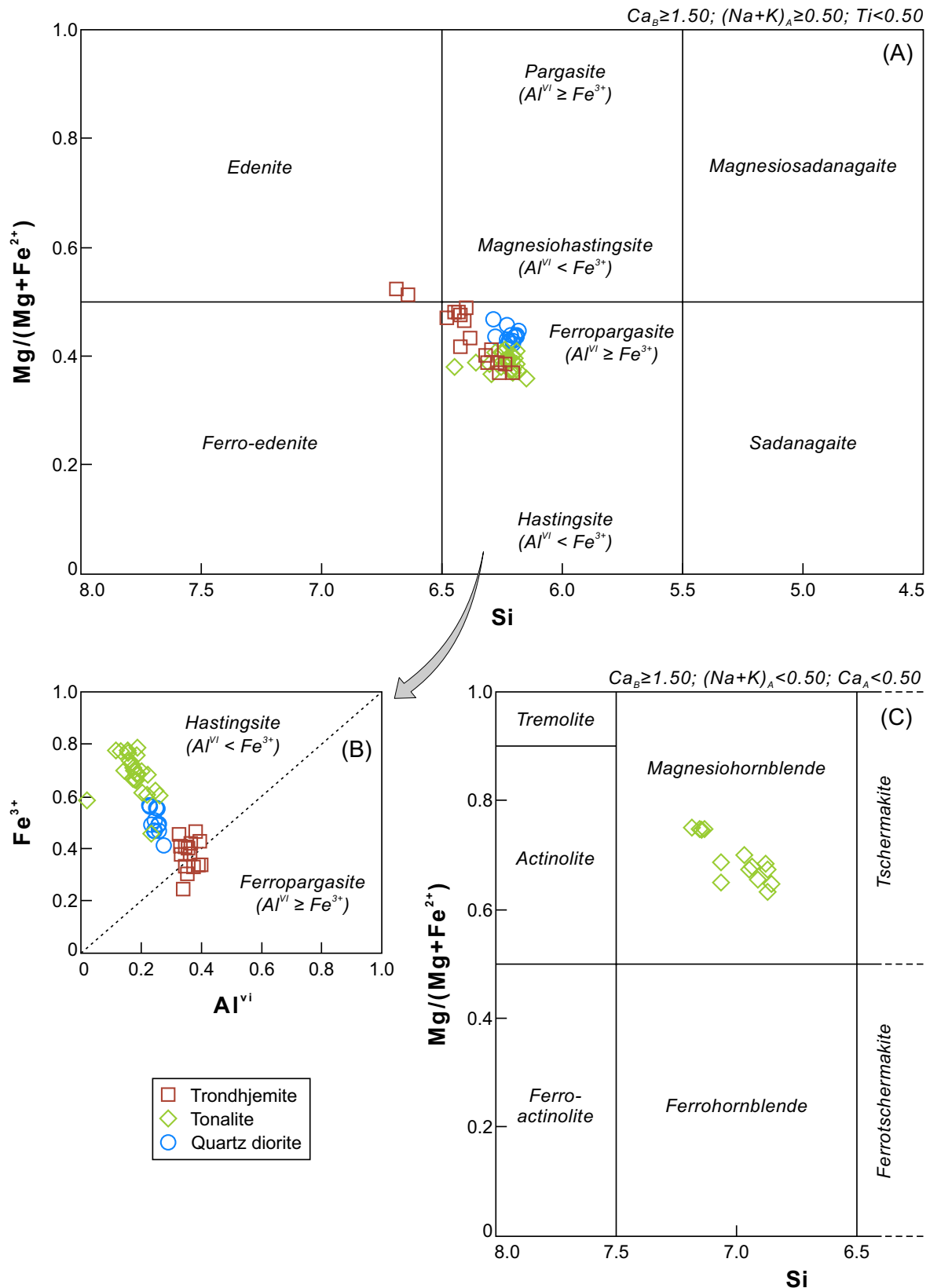


Figure 6. Classification diagrams for amphibole after Leake *et al.* (1997). (A) $Mg/(Mg + Fe^{2+})$ versus Si diagram based on $Ca_B \geq 1.50$, $(Na + K)_A \geq 0.50$, and $Ti < 0.50$. (B) Al^{VI} versus Fe^{3+} diagram to discriminate ferropargasite ($Al^{VI} \geq Fe^{3+}$) from hastingsite ($Al^{VI} < Fe^{3+}$) according to diagram (A). (C) $Mg/(Mg + Fe^{2+})$ versus Si diagram based on $Ca_B \geq 1.50$, $(Na + K)_A < 0.50$, and $Ca_A < 0.50$.

Crystallization parameters

The mineral chemical data presented in the supplementary tables for the main silicate minerals of the Café enderbite (plagioclase, biotite, amphibole and pyroxene) were used to constrain the temperature, pressure, oxygen fugacity and

water content conditions that prevailed during the crystallization of these rocks. Early magmatic minerals not affected by post-magmatic processes were selected. The calculations of the intrinsic parameters from mineral chemical data were performed using the WinAmptb software (Yavuz and Döner

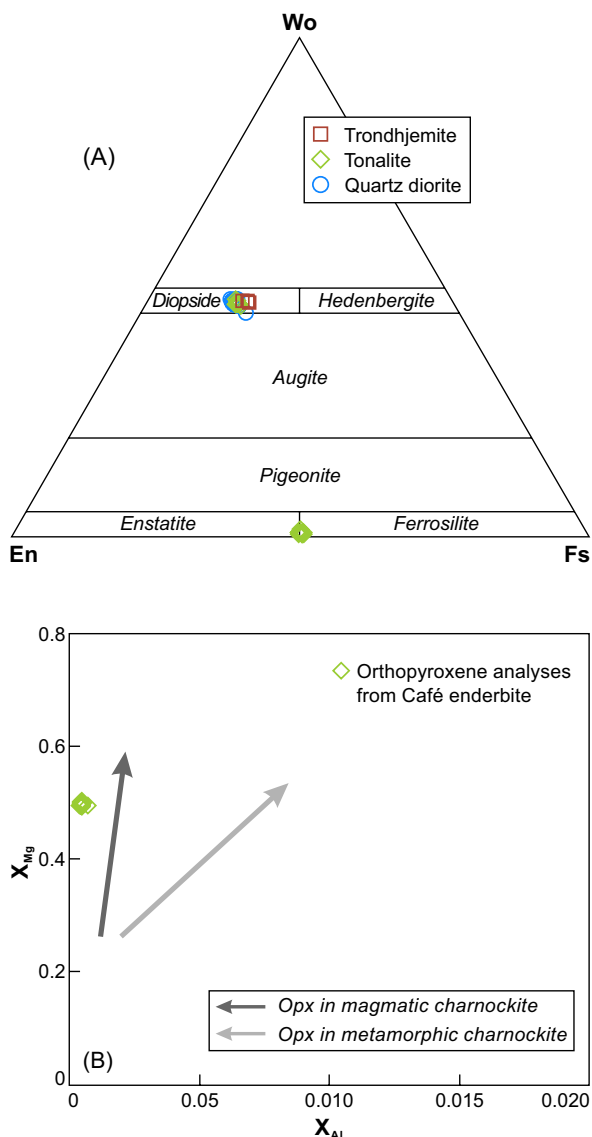


Figure 7. Plots of pyroxene compositions showing (A) En-Wo-Fs classification diagram after Morimoto *et al.* (1988) and (B) X_{Mg} [=Mg/(Fe + Mg)] versus X_{Al} (=Al/2) diagram with orthopyroxene chemical analyses from the Café enderbite. Arrows in (B) indicate the compositional trends of orthopyroxene in igneous and metamorphic rocks after Rajesh *et al.* (2011).

2017) for amphibole and plagioclase, the WinPyrox software (Yavuz 2013) for pyroxene, and the Geo- fO_2 software (Li *et al.* 2019) for biotite. Temperatures based on zircon and apatite saturation were also estimated from whole-rock analyses performed by Marangoanha *et al.* (2019a) using the GCDkit software (Janoušek *et al.* 2003). The calculated parameters used to estimate the crystallization conditions are summarized in Tab. 2.

Temperature

The use of different geothermometers yielded a wide range of temperatures for the rocks from the Café enderbite (cf. Tab. 2). Geothermometers of zircon and apatite saturation proposed by Watson and Harrison (1983) and Harrison and Watson (1984), respectively, provided temperature intervals of 885–607 and 964–553°C for each corresponding calibration. The highest temperatures obtained from the zircon

saturation geothermometer are supported by the occurrence of early crystallized euhedral zircon crystals included in feldspars, ferromagnesian minerals, and Fe–Ti oxides. Calibration models based on biotite composition display different values: Luhr *et al.*'s (1984) geothermometer records values between 1,026 and 949°C, while the graphical thermometer proposed by Henry *et al.* (2005) indicates temperatures between ~750 and 680°C (Fig. 8A). Amphibole-only geothermometers display temperatures of 834–782°C according to the calibration of Putirka (2016) and 918–833°C calculated with the calibration equation of Ridolfi *et al.* (2010). These temperatures are close to the values recorded by the calculated temperature for the amphibole–plagioclase pair proposed by Holland and Blundy (1994), which lie within the range of 919–693°C. A clinopyroxene-based thermometer from Molin and Zanazzi (1991) provided temperatures ranging from 906 to 862°C, while Putirka's (2008) calibration displayed higher values between 1,152 and 1,104°C for this same thermometer.

Most of these temperatures attributed to the Café enderbite reveal values of ~950–850°C that appear to be rather consistent with the near-liquidus temperatures expected for most granitoids from the charnockite series (Weiss and Troll 1989, Frost *et al.* 1999, Bucher and Frost 2006, Frost and Frost 2008), whereas the calculated highest temperatures (~1,150–1,100°C) are not discarded since many charnockitic occurrences worldwide have recorded liquidus temperatures higher than 1,100°C (Fuhrman *et al.* 1988, Kolker and Lindsley 1989, Weiss and Troll 1989, Young *et al.* 1997). Minor underestimated temperatures of ~600–550°C, obtained mainly by zircon and apatite saturation methods, could indicate that these rocks did not reach the Zr and P saturation levels or even that zircon crystallized late (at lower temperature) in more mafic rocks.

Pressure

Although the cores and rims of amphibole crystals in the studied rocks do not show any significant compositional variation, the pressure is estimated using only the composition of their rims, which indicates pressure conditions at near-solidus temperatures (cf. Tab. 2). Geobarometric estimates for these rocks could be attempted mainly on the basis of Al total content in amphibole. Following this method, the geobarometers of Hammarstrom and Zen (1986), Hollister *et al.* (1987), and Schmidt (1992) provided similar pressures, ranging from 756 to 391 MPa, while those obtained by the calibrations of Johnson and Rutherford (1989) and Mutch *et al.* (2016) tend to be slightly lower and record values varying between 597 and 312 MPa. The amphibole-only barometer proposed by Ridolfi *et al.* (2010) yielded pressures even lower than those from the above calibrations, with values of 440–180 MPa. On the other hand, Anderson and Smith's (1995) graphical geobarometer (Fig. 8B) presented comparatively similar values of pressure ranging from ~750 to 150 MPa, which overlap those obtained with the other calibration equations (cf. Tab. 2).

In general, the barometric data can be separated into two groups discriminating different pressures, which can be clearly seen in Fig. 8B. Higher pressures of ~750–600 MPa

Table 2. Summary of crystallization parameters for the Café enderbite.

Calibration	Quartz diorite	Opx-tonalite	Opx-trondhjemite
Temperature (°C)			
Watson and Harrison (1983) – Zircon saturation	607	885	853
Harrison and Watson (1984) – Apatite saturation	553	964	778
Luhr <i>et al.</i> (1984) – Biotite	-	1026	949
Putirka (2016) – Amphibole	834–817	807–782	817–782
Ridolfi <i>et al.</i> (2010) – Amphibole	918–897	896–873	912–833
Holland and Blundy (1994) – Amphibole–plagioclase	877–808	919–777	781–693
Molin and Zanazzi (1991) – Clinopyroxene	904–899	906–862	904–903
Putirka (2008) – Clinopyroxene	1152–1132	1148–1104	1134–1125
Pressure (MPa)			
Hammarstrom and Zen (1986) – Al-in-hornblende	643–583	621–546	706–391
Hollister <i>et al.</i> (1987) – Al-in-hornblende	685–617	660–576	756–401
Schmidt (1992) – Al-in-hornblende	679–621	658–587	738–440
Johnson and Rutherford (1989) – Al-in-hornblende	525–474	506–443	578–312
Mutch <i>et al.</i> (2016) – Al-in-hornblende	540–488	520–458	597–342
Ridolfi <i>et al.</i> (2010) – Amphibole	371–312	347–280	444–180
Continental depth (km)			
Ridolfi <i>et al.</i> (2010)	14–12	13–11	17–7
Schmidt (1992)	26–23	25–22	28–17
Oxygen fugacity – NNO buffer (log fO_2)			
Fegley (2013)	–9.9 to –10.4	–10.4 to –11.2	–9.1 to –11.3
Ridolfi <i>et al.</i> (2010)	–12.2 to –12.4	–12.6 to –13.2	–12.4 to –13.1
H₂O_{melt} (wt.%)			
Ridolfi <i>et al.</i> (2010)	5.4–5.0	5.5–4.8	5.6–5.0

would indicate the initial magma generation under deep conditions (depths of ~28–17 km; cf. Tab. 2). This result is consistent with the origin of the Café enderbite rocks from the partial melting of mafic granulite under lower crustal conditions (Marangoanha *et al.* 2019a). On the other hand, the lower pressures of 500–180 MPa should correspond to the emplacement conditions at shallower levels but still at mid-high crustal depths (~14–11 km, corresponding to the mesozone; cf. Tab. 2); according to Marangoanha *et al.* (2019a), this magma was channeled through the crust via shear zones under a transpressional tectonic regime, and the mylonitic texture of these rocks may explain such conditions. The mylonitic texture on the ~2.74-Ga-old granitoids from Carajás Province is supported by the syntectonic nature of their plutons (Barros *et al.* 2009, Feio *et al.* 2012, Dall'Agnol *et al.* 2013, Oliveira *et al.* 2018, Marangoanha *et al.* 2019a, 2019b, Félix *et al.* 2020).

It is also worth highlighting the importance of the results obtained by the P–T diagram from Ridolfi *et al.* (2010; Fig. 8C). The findings reveal that the amphiboles from the Café enderbite plot within domain 1 (Mg-Hbl + Pl ± Opx ± Mt ± Ilm ± Bt) and mostly within domain 2 (Tsc-Prg + Pl ± Cpx ± Opx ± Mt ± Ilm), which completely matches the main mineral phases in the studied rocks, including plagioclase, quartz, biotite, amphibole, clinopyroxene, orthopyroxene, magnetite, and ilmenite (cf. Tab. 1).

Oxygen fugacity

Biotite and amphibole are particularly good sensors for the oxidation state of the magma from which they crystallized (Ridolfi *et al.* 2010, Fegley 2013, Hossain and Tsunogae 2014) because their chemical compositions can reflect oxidation conditions during magma crystallization. In other words, as fO_2 increases in magmatic systems, the Fe^{3+}/Fe^{2+} ratio in the melt increases, leaving progressively less Fe^{2+} to compete with Mg^{2+} for site occupancy in mafic minerals and thus increasing the Mg# in these minerals (Wones and Eugster 1965). Therefore, high Mg contents in mafic minerals appear to be characteristic of high fO_2 magmas. In this sense, biotite and amphibole were used to estimate the oxygen fugacity to constrain the crystallization conditions of the rocks from the Café enderbite.

The Café enderbite exhibits moderate FeOt/(FeOt + MgO) ratios in whole-rock analyses, ranging between 0.56 and 0.76 (except for one sample with 0.86; see Marangoanha *et al.* 2019a). Accordingly, this pattern is reflected in the biotite and amphibole compositions, which also present moderate Fe/(Fe + Mg) ratios ranging from 0.42 to 0.52 and from 0.34 to 0.70, respectively (Suppl. Tabs. B and C). The Fe/(Fe + Mg) versus Al^{IV} diagram from Anderson and Smith (1995) shows that the analyzed amphiboles plot in the fields of intermediate and high fO_2 (Fig. 9A), and in the Fe/(Fe + Mg) versus Al^{IV} + Al^{VI} diagram (Fig. 9B), the biotites plot in the magnetite series granite field from Anderson *et al.* (2008). These results are in agreement

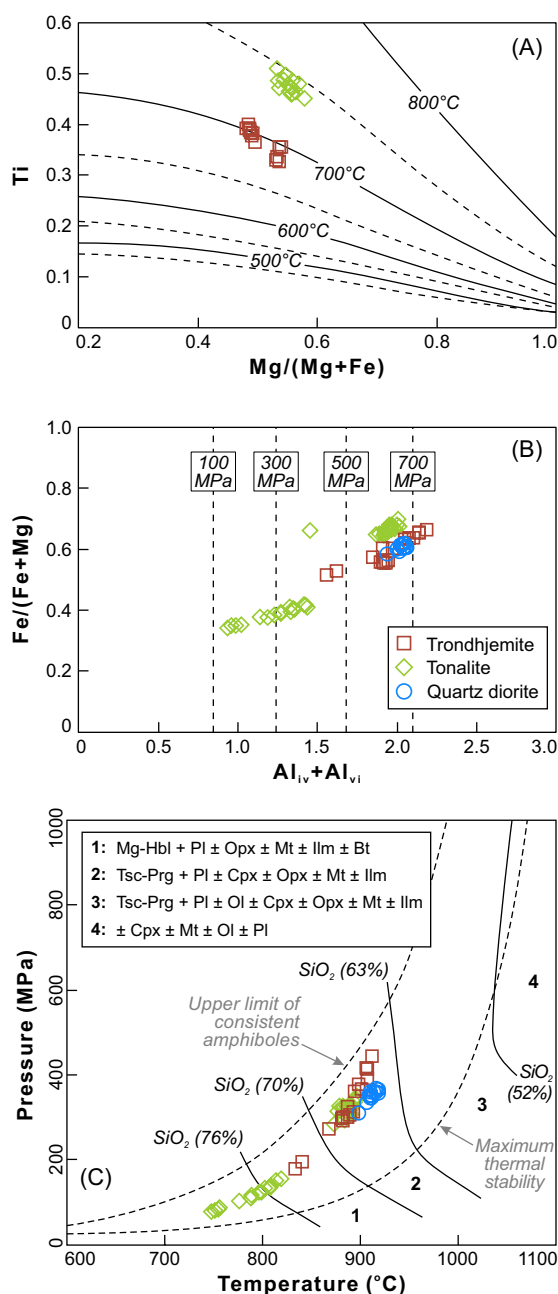


Figure 8. (A) Ti versus Mg/(Mg+Fe) diagram of biotite compositions, where the solid curves are temperature isotherms (°C) calculated from the surface-fit equation after Henry *et al.* (2005) and the dashed curves are the intermediate 50°C interval isotherms. (B) Fe/(Fe+Mg) versus Al^{IV}+Al^{VI} diagram for amphiboles from the studied rocks, with isobars from Anderson and Smith (1995) based on Schmidt (1992), showing possible crystallization pressure ranges of amphibole. (C) P-T diagram for calcic amphiboles in the studied enderbites calculated after Ridolfi *et al.* (2010). The maximum relative P errors range from 11% (at the maximum thermal stability curve) to 25% (at the upper limit of consistent amphiboles). The isopleths (black solid lines) represent the anhydrous SiO₂ content (wt.%) of the melt, and the P-T stability limits constrain the equilibrium of phases such as biotite (Bt), plagioclase (Pl), orthopyroxene (Opx), clinopyroxene (Cpx), magnetite (Mt), ilmenite (Ilm), and olivine (Ol) with amphiboles (Mg-Hbl = magnesiohornblende; Tsc-Prg = tschermakitic pargasite).

with the presence of subhedral magnetite in the studied rocks (cf. Fig. 3F) and indicate that the Café enderbite crystallized under high fO_2 conditions, analogous to the granites of the magnetite series from Ishihara (1981). Estimation of the oxygen fugacity at the NNO buffer ($\log fO_2$) based on amphibole

compositions from Fegley (2013) provides values varying from -11.3 to -9.1 for the studied rocks. Ridolfi *et al.*'s (2010) calibration under these same conditions yields slightly lower values ranging between -13.2 and -12.2 (cf. Tab. 2). Most amphibole compositions, when plotted on the $\log fO_2$ -T diagram after Ridolfi *et al.* (2010), indicate that the Café enderbite evolved under relatively oxidizing conditions, on or slightly above the fayalite-magnetite-quartz (FMQ) buffer; additionally, some analyses plot on and above the nickel-nickel oxide (NNO) buffer and below the NNO+2 buffer, describing comparatively more oxidizing conditions (Fig. 9C). Therefore, the presence of primary magnetite (cf. Fig. 3F), the relatively high Mg contents in biotite and amphibole (cf. Figs. 9A and 9B), and the fO_2 values (cf. Tab. 2) all strongly suggest that these rocks crystallized under oxidized conditions.

Water content

Experimental data for granitic systems have demonstrated that Ca-amphibole crystallization is extremely dependent on the water (H_2O_{melt}) and CaO contents in magma and requires a minimum H_2O_{melt} of 4 wt.% at 200–400 MPa to stabilize this mineral at magmatic temperatures (Naney 1983, Dall'Agnol *et al.* 1999, Klimm *et al.* 2003, Bogaerts *et al.* 2006). Furthermore, the Al^{VI} content in this mineral is sensitive to the H_2O content in the melt and can be used to estimate the stability field of amphibole crystallization. Therefore, the H_2O_{melt} concentrations calculated from Ridolfi *et al.*'s (2010) hygrometric equation for amphibole in the rocks from the Café enderbite display values varying from 4.8 to 5.6 wt.% (cf. Tab. 2). A comparison of these H_2O_{melt} values with amphibole temperatures (T- H_2O_{melt} diagram after Ridolfi *et al.* 2010) clearly reveals that the stability field of amphibole crystallization was reached under such magmatic conditions (Fig. 9D).

Experimental works from Naney (1983), Prouteau and Scaillet (2003), and Oliveira *et al.* (2010) have demonstrated that 5 wt.% H_2O_{melt} at 400 MPa or 7–9 wt.% H_2O_{melt} at 960 MPa is required for amphibole to be the silicic liquidus phase and mainly to inhibit pyroxene formation. Based on this outcome, the presence of orthopyroxenes and clinopyroxenes as common mineral phases in the studied rocks (≤ 12 and ≤ 22 vol.%, respectively; cf. Tab. 1) can plausibly imply that the stability fields of these minerals were attained; this interpretation is supported by the relatively low H_2O_{melt} content and moderate- to high-pressure conditions recorded for these rocks (4.8–5.6 wt.% and 750–600 MPa, respectively; cf. Tab. 2).

DISCUSSION

Petrogenetic process

Introduction

As noted previously, the origin (as well as the concept) of charnockites *lato sensu* is still a matter of discussion, since many authors have proposed different — and opposing — models to

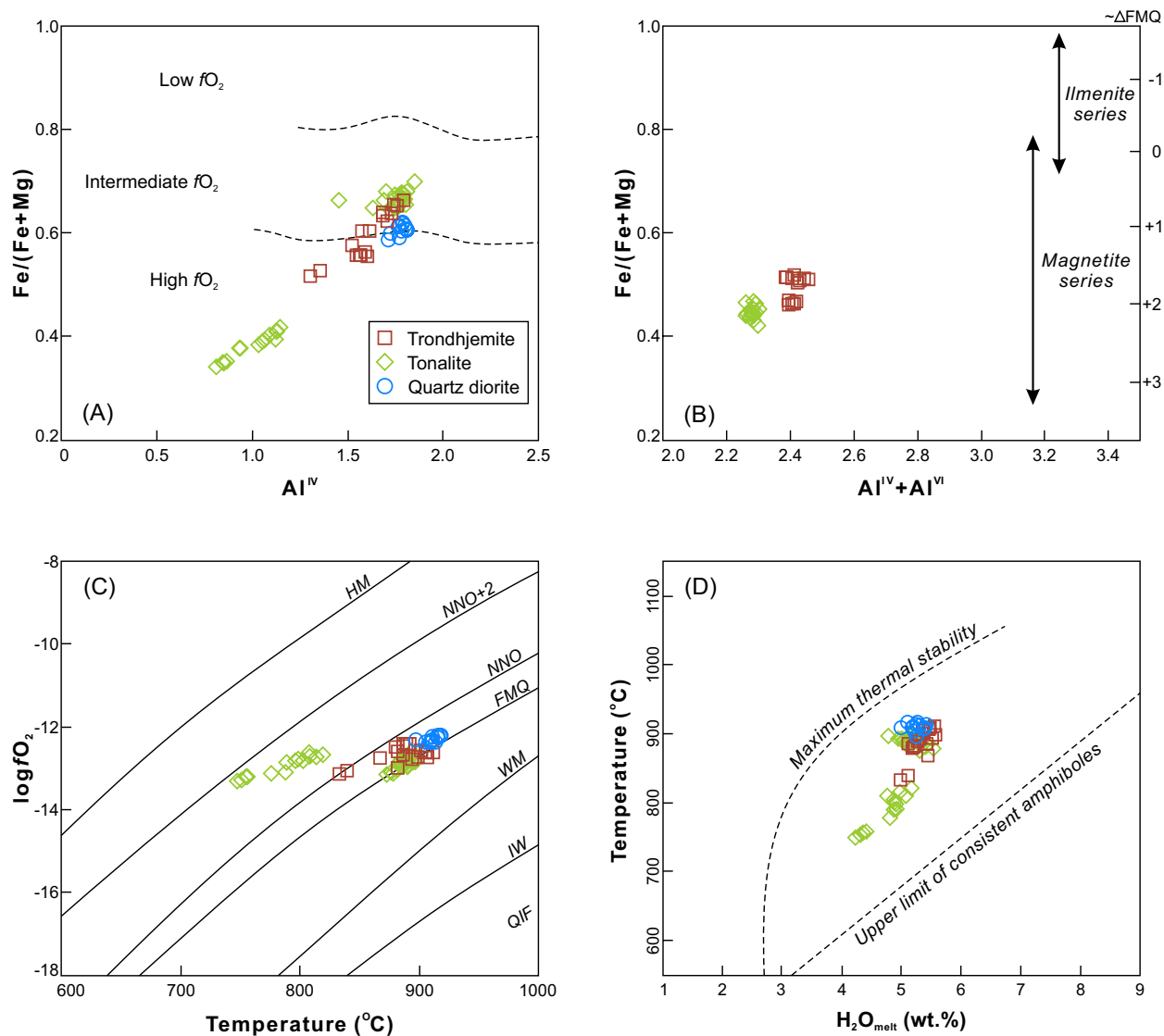


Figure 9. (A) $\text{Fe}/(\text{Fe} + \text{Mg})$ versus Al^{IV} diagram showing the compositional variations of amphibole for the studied enderbites (low, intermediate, and high $f\text{O}_2$ fields according to Anderson and Smith 1995). (B) $\text{Fe}/(\text{Fe} + \text{Mg})$ versus $\text{Al}^{\text{IV}} + \text{Al}^{\text{VI}}$ diagram showing the compositional variations in biotite for the studied rocks. Variation in $\text{Fe}/(\text{Fe} + \text{Mg})$ in the ilmenite and magnetite series and ΔFMQ values are from Anderson *et al.* (2008). (C) Amphibole compositions from the Café enderbite plotted on the $\log f\text{O}_2$ versus T diagram (after Ridolfi *et al.* 2010). (D) T versus $\text{H}_2\text{O}_{\text{melt}}$ diagram using the calculation scheme by Ridolfi *et al.* (2010).

generate such rocks (Pichamuthu 1969, Newton 1992, Rajesh 2007, Frost and Frost 2008, Rajesh and Santosh 2012 and references therein). Considering only the igneous origin (Frost and Frost 2008 and references therein), the most relevant proposals, as listed by Rajesh (2007), are as follows: partial melt from mafic lower crustal granulite (Duchesne *et al.* 1989, Longhi *et al.* 1999, Marangoanha *et al.* 2019a) or a trace element-enriched mantle source (Icenhower *et al.* 1998); extensive fractionation of Fe–Ti-rich ferrodiorite magma (Vander Auwera *et al.* 1998, Scoates and Lindsley 2000); or even residues or cumulates after the removal of an evolved (granitic) melt (Emslie 1991, Mitchell *et al.* 1996, Markl and Höhndorf 2003).

Origin and geochemical modeling

The rocks of the Café enderbite display petrographic, geochemical, and isotopic characteristics that allow us to constrain the petrogenetic processes involved in their evolution. Marangoanha *et al.* (2019a) made important contributions

to understanding these rocks, and they established, based on petrological data, that the initial magma of the Café enderbite (quartz dioritic composition — sample BVD 35-A) was generated from 21% melting of a Mesoarchean mafic lower crust, leaving a residue composed of plagioclase, clinopyroxene, orthopyroxene, and magnetite. Furthermore, these authors showed that these rocks display a wide geochemical spectrum (Tab. 3), with an emphasis on SiO_2 presenting values ranging between 53.00 and 80.40 wt.% and on the Mg number [$\text{Mg}\# = \text{Mg}/(\text{Mg} + \text{Fe}^{2+})$], which varies from 0.36 to 0.63 (with an outlier value of 0.22).

Additionally, the contrasting behaviors of compatible and incompatible elements in mineral phases provide a useful tool to evaluate whether magmatic evolution was controlled by fractional crystallization, partial melting, or more complex processes (Hanson 1978, 1989, Rollinson 1993, Dall'Agnol *et al.* 1999). In general, Sr and Ba present a positive correlation in the studied rocks; these elements

Table 3. Average major and trace element compositions of the Café enderbite varieties (complete data in Marangoanha *et al.* 2019a).

Variety	Quartz diorite		Orthopyroxene tonalite		Orthopyroxene trondhjemite	
Number of samples (N)	(N = 2)		(N = 6)		(N = 4)	
Statistical data	Average	St. dev.	Average	St. dev.	Average	St. dev.
Major elements (wt.%)						
SiO ₂	54.80	2.55	69.15	2.12	77.13	4.70
TiO ₂	1.31	1.22	0.78	0.25	0.19	0.29
Al ₂ O ₃	14.63	1.45	13.63	0.57	11.53	1.32
Fe ₂ O ₃ *	5.19	1.47	3.87	0.93	1.92	1.14
MnO	0.05	0.00	0.04	0.01	0.02	0.02
MgO	4.00	0.56	1.91	0.71	0.62	0.69
CaO	10.23	0.32	3.83	0.69	2.42	0.92
Na ₂ O	6.71	0.57	5.03	0.60	4.63	0.22
K ₂ O	0.67	0.11	0.76	0.45	0.57	0.02
P ₂ O ₅	0.02	0.01	0.03	0.11	0.01	0.00
Trace elements (ppm)						
Ba	84	18	302	227	199	41
Sr	339	46	308	145	288	22
Rb	3.8	0.5	18.7	13.9	8.3	2.3
Zr	103	99	353	234	315	40
Y	29.8	8.3	15.3	3.0	24.0	8.5
Hf	2.8	2.5	9.4	5.6	9.4	1.6
Nb	20.5	16.5	13.1	5.3	13.8	1.5
Ta	0.9	0.4	1.2	0.4	1.0	0.8
Th	0.8	0.8	10.5	4.2	10.7	3.4
La	12.9	5.1	14.6	14.5	8.4	1.5
Ce	26.3	8.8	23.3	24.3	18.0	0.9
Pr	3.45	0.39	2.63	2.59	2.51	0.44
Nd	15.6	0.1	10.8	7.4	11.6	2.8
Sm	4.74	0.74	2.83	0.85	2.64	0.78
Eu	0.90	0.04	1.02	0.14	1.11	0.10
Gd	5.38	1.05	2.67	0.60	3.07	1.09
Tb	0.88	0.20	0.44	0.10	0.56	0.14
Dy	5.41	1.25	2.83	0.65	3.50	0.97
Ho	1.08	0.31	0.57	0.11	0.77	0.25
Er	3.28	0.69	1.67	0.37	2.59	0.83
Tm	0.46	0.06	0.27	0.04	0.42	0.12
Yb	2.97	0.34	1.72	0.38	2.81	0.89
Lu	0.51	0.07	0.26	0.06	0.47	0.17
Mg#	0.61	0.04	0.52	0.12	0.39	0.06
Eu/Eu*	0.54	0.07	1.03	0.27	1.14	0.46

Fe₂O₃*: total iron recalculated as Fe₂O₃; Mg# = Mg/(Mg + Fe); Eu/Eu* = Eu_N/[(Sm_N + Gd_N)/2]; St. dev.: standard deviation.

vary widely, increasing from the less to the more evolved rock (Fig. 10A). The same pattern is observed in the Sr versus Rb diagram (Fig. 10B), in which Rb behaves similarly to Ba and displays a positive correlation with Sr. The Sr/Ba versus Rb/Sr diagram shows that Sr/Ba values decrease from the less to the more evolved sample as Rb/Sr values increase, forming a clear negative correlation (Fig. 10C). These diagrams reveal that the tonalitic and trondhjemitic rocks present equivalent

trends, where the tonalites have a wider range that encompasses the trondhjemite trend.

The observed systematic variations in major and trace elements following linear trends (Marangoanha *et al.* 2019a), associated with large variations in Rb, Sr, Ba, Sr/Ba, and Rb/Sr, indicate that fractional crystallization could have played an important role in the magmatic evolution of these rocks. This inference is supported by the observed wide range of

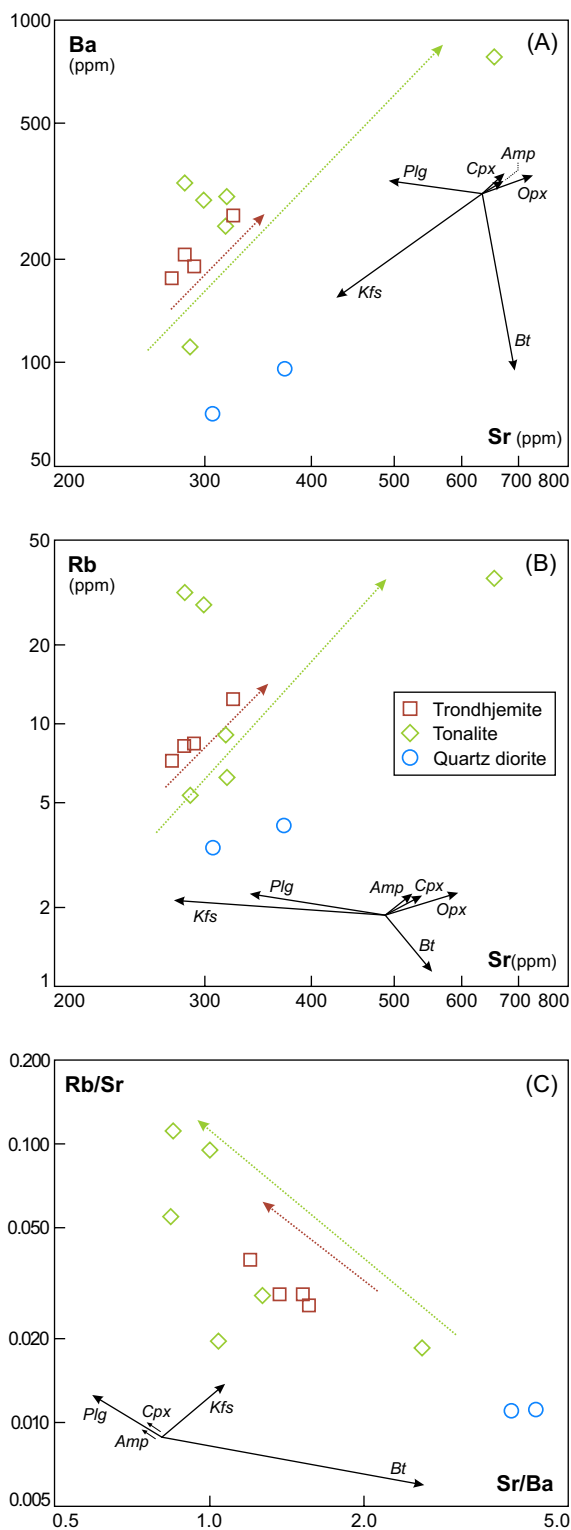


Figure 10. Log-log fractional crystallization vector diagrams: (A) Sr versus Ba, (B) Sr versus Rb, and (C) Sr/Ba versus Rb/Sr. The vectors indicate the influence of fractionation of plagioclase (Plg), potassium feldspar (Kfs), biotite (Bt), amphibole (Amp), clinopyroxene (Cpx), and orthopyroxene (Opx) on the composition of the residual liquids. The dotted arrows show possible trends during fractional crystallization into tonalites and trondhjemites.

Mg number, which are interpreted to be strongly influenced by fractional crystallization (Roeder and Emslie 1970, Best and Christiansen 2001). Therefore, fractional crystallization processes were investigated using major and trace element modeling.

Owing to the broad SiO₂ and Mg# intervals that form the quartz dioritic–tonalitic–trondhjemitic series as well as the Rb–Ba–Sr behavior in the tonalitic and trondhjemitic varieties, two fractional crystallization stages were assumed:

- the first stage was represented by an orthopyroxene-bearing tonalitic magma generated from a quartz dioritic liquid (quartz diorite→orthopyroxene tonalite);
- later, an orthopyroxene-bearing trondhjemitic magma derived from a previously formed orthopyroxene-bearing tonalitic liquid (orthopyroxene tonalite→orthopyroxene trondhjemite).

The mineral assemblages involved during the two stages of fractional crystallization were chosen by the vector diagrams from Fig. 10.

To evaluate this hypothesis quantitatively, major element mass balance calculations were performed using the GENESIS version 4.0 software (Teixeira 2005). This method consists of adjusting the relative proportions of fractionating minerals from the source (initial melt) to reproduce the composition of the expected melt. The quality of the model is reliable if the sum of the square residuals (ΣR^2) is ≤ 1.2 (Wyers and Barton 1986), allowing us to proceed to trace element modeling using Excel sheets created by the authors of the present work based on the Rayleigh equation for fractional crystallization (Rayleigh 1896; Eq. 1):

$$C_L/C_0 = F^{(D-1)} \tag{1}$$

Where:

C_L and C_0 : the trace element composition of the remaining liquid phase during fractional crystallization (daughter) and the initial trace element composition of the magma (parent), respectively;

F: the mass fraction of residual magma relative to the initial mass;

D: the bulk partition coefficient for the fractionating mineral assemblage.

The mineral/liquid partition coefficients (Kd) used in the modeling were obtained from Rollinson (1993) and the online database <https://earthref.org/KDD/>, given in Suppl. Tab. E.

In the first stage of the modeling, sample BVD 35-A (quartz diorite) was taken to represent the parental melt composition, which was proposed by Marangoanha *et al.* (2019a) as the initial liquid formed by partial melting of a mafic granulite. Sample BVD 52-A was assumed to be the daughter because it represents one of the less evolved samples in the tonalitic variety and gives more consistent results. Although the vectors in Figs. 10A-10C show that the tonalites were formed by fractionating plagioclase, orthopyroxene, clinopyroxene, and amphibole, the lowest sum of the squared residuals ($\Sigma R^2 = 0.308$; Tab. 4) is obtained when amphibole is replaced by magnetite; hence, the fractionating phases, composed of 69.76% plagioclase, 28.65% clinopyroxene, 1.52% magnetite, and 0.07% orthopyroxene, yield a liquid (daughter) to cumulate ratio of 8:92. The same proportions of liquid and fractionating phases were tested in the trace element modeling (Fig. 11A; cf. Tab. 4), which also

Table 4. Modeling major and trace element compositions and fractionated mineral assemblages for generation of the tonalitic variety of the Neoproterozoic Café enderbite by fractional crystallization.

	BVD 35-A	Cumulate	Composition of minerals				Calculated liquid (C _L) [']	BVD 52-A
	(C ₀) ^a	(C _s)	Pl ^c	Cpx ^c	Mt ^d	Opx ^c		(C _L) ^a
	Quartz diorite ^b	Bulk						69.76%
Major elements (wt.%)								
SiO ₂	57.80	56.85	57.19	54.16	0.00	51.93	69.68	69.75
TiO ₂	0.45	0.02	0.02	0.02	0.00	0.07	1.13	0.76
Al ₂ O ₃	15.98	16.00	21.93	0.50	0.00	0.18	14.00	13.85
FeO*	3.81	3.97	0.05	8.39	100.00	28.86	2.65	2.71
MnO	0.05	0.05	0.00	0.17	0.00	0.90	0.03	0.03
MgO	3.68	3.82	0.00	13.34	0.00	16.93	1.78	1.76
CaO	10.21	10.68	5.59	23.24	0.00	0.49	5.26	5.30
Na ₂ O	7.26	7.83	10.63	0.49	0.00	0.05	4.98	5.35
K ₂ O	0.76	0.78	1.08	0.01	0.00	0.00	0.49	0.49
Trace elements (ppm)								
Ba	96.3						188.3	250.0
Rb	4.1						14.7	9.0
Sr	371.0						304.2	317.0
Y	35.6						25.0	16.5
Zr	33.0						329.0	324.0
Nb	8.8						11.1	12.0
La	9.30						14.21	14.40
Ce	20.00						22.17	23.10
Nd	15.50						10.43	10.20
Sm	5.26						4.13	2.91
Eu	0.92						1.02	0.95
Gd	6.12						4.05	3.29
Yb	3.21						1.45	1.74
Lu	0.560						0.296	0.330

ΣR²=0.308.

FC=92%.

ΣR²: Sum of the squared residuals; FC: Fractional crystallization. All iron is reported as FeO; ^aBulk composition from Marangoanha *et al.* (2019a); ^bOriginal oxide values recast to 100%; ^cMineral composition values from this work; ^dMineral composition values from Deer *et al.* (1992).

presented a good fit between the calculated liquid (generated by fractional crystallization from quartz diorite — sample BVD 35-A) and the representative tonalite (BVD 52-A). This high fractionation of 92% of the initial liquid is probably overestimated and its meaning is discussed later.

The next stage of the modeling represents the fractional crystallization of a tonalitic melt (freshly formed in the first stage; sample BVD 52-A) to generate a trondhjemite. Assuming the composition of sample ED 1 as the daughter, the best model was obtained by fractionating plagioclase (71.43%), clinopyroxene (21.46%), orthopyroxene (4.55%), and amphibole (2.56%), which represents the same fractionating assemblage indicated by the vectors in Fig. 10. In this model, the fractionating assemblage corresponds to 45% of the initial liquid, and the sum of the squared residuals is relatively low (ΣR² = 0.565; Tab. 5). This model also gives an excellent fit for trace element modeling (Fig. 11B; cf. Tab. 5).

Alternative processes

Despite the aforementioned modeling, we have also examined whether the mechanism of fractional crystallization could have proceeded with simultaneous crustal assimilation to generate the Café enderbite. As the crust of Carajás Province shows a complex evolution that involves multiple episodes of magmatism, metamorphism, hydrothermalism, and deformation, these processes are reflected in its heterogeneous composition, as displayed in Fig. 1C. Therefore, we tested assimilation-fractional crystallization (AFC) involving three different crustal compositions:

- mafic crust, represented by an amphibolite from Souza *et al.* (2017);
- intermediate crust, composed of the Ouro Verde tonalitic granulite (Marangoanha *et al.* 2019a);
- felsic crust, represented by the Cruzadão granite (Feio *et al.* 2013).

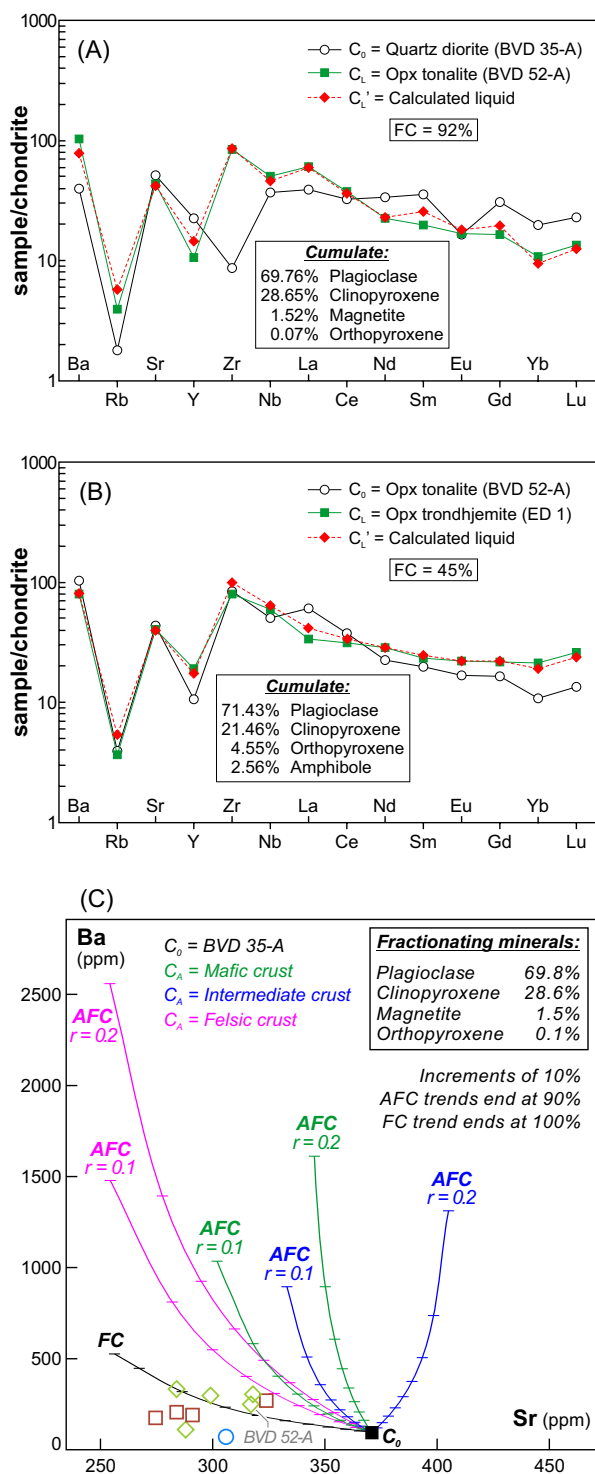


Figure 11. Fractional crystallization (FC) modeling (trace elements) to differentiation of the (A) opx-tonalite (daughter) from the quartz diorite (parent) in stage 1 and (B) opx-trondhjemite (daughter) from the opx-tonalite (parent) in stage 2. FC is percentage of fractional crystallization. Chondrite (C1) normalization values are from McDonough and Sun (1995). Trace element data are given in Tabs. 4 (stage 1) and 5 (stage 2). (C) Sr versus Ba diagram showing the results of assimilation-fractional crystallization (AFC) and FC modeling. In (C), we used the PETROMODELER software from Ersoy (2013) based on equations from DePaolo (1981). The mafic, intermediate, and felsic crust compositions are taken from Souza *et al.* (2017), Marangoanha *et al.* (2019a), and Feio *et al.* (2013), respectively. “r” denotes the ratio between the volumes of crustal assimilation and FC ($r = m_a/m_c$). The Sr and Ba contents of the respective assimilant compositions (C_A) and the starting composition (C_0) and the mineral/liquid partition coefficients (Kd) for each mineral are given in Suppl. Tab. F. Symbols as in Fig. 10.

In this model, we evaluated the interaction between the starting composition (C_0) represented by the initial liquid in the modeling of the first stage (quartz dioritic composition; sample BVD 35-A) with the same fractionating assemblage and the assimilant compositions (C_A) listed above (mafic, intermediate, and felsic crust), with assimilation rates of 10 and 20% ($r = 0.1$ and $r = 0.2$, respectively). The results (Fig. 11C) clearly exclude the involvement of AFC process in generating the studied rocks and furthermore display an excellent fit to fractional crystallization process, as previously tested.

Comparison with other charnockites from Carajás Province and cratons worldwide

Although the vast majority of continental crust is composed of amphibole- and/or biotite-bearing granitoids, orthopyroxene-bearing granitoids form a minor but equally important component of the middle and lower continental crust and played a crucial role in the formation and evolution of the Precambrian crust (Rajesh and Santosh 2012 and references therein). Carajás Province (Amazonian craton, northern Brazil) is a good example of this feature; here, all occurrences of rocks from the charnockitic series (admitting an ‘igneous’ origin according to Frost and Frost 2008) are restricted to the Neoproterozoic (ca. 2.74 Ga), are relatively well preserved, and reveal significant information concerning geological setting, tectonic regime, intrinsic crystallization conditions, and other factor that contribute to understanding the Archean evolution of this province. In addition to the Café enderbite, they are also represented by the Pium diopside-norite (Vasquez *et al.* 2008, Feio *et al.* 2012, Santos *et al.* 2013) and an orthopyroxene-bearing granodiorite with spatially associated gabbro-norites (Félix *et al.* 2020).

Therefore, we have gathered a data set containing the crystallization parameters of some charnockite occurrences worldwide to establish a general comparison between them and the studied rocks, highlighting the similarities and differences related to this peculiar magmatism. The dataset is presented in Tab. 6. These data reveal that most temperatures record high values, generally > 1,000°C, for the analyzed charnockites, whereas the Matok pluton (Limpopo Belt, South Africa) and Louis Lake batholith (Wyoming Province, USA) exhibit temperatures between ~900 and 800°C but are still high. Concerning the estimated pressure, most of the charnockites present high to relatively moderate values, ranging from 900 to 400 MPa; the exceptions are the orthopyroxene-bearing granodiorites from the Ourilândia do Norte region (Carajás Province, northern Brazil) displaying moderate to low pressures of 310–190 MPa and subordinate analyses from the Matok pluton. The available oxygen fugacity data strongly suggest a tendency for charnockitic magma to crystallize under oxidizing conditions between the FMQ and NNO+2 buffers (cf. Tab. 6), although Frost and Frost (2008) pointed out wide ranges of oxygen fugacity from reducing conditions below the FMQ buffer to oxidizing conditions with $\Delta \log \text{FMQ} > +2$.

Table 5. Modeling major and trace element compositions and fractionated mineral assemblages for generation of the trondhjemitic variety from the Neoproterozoic Café enderbite by fractional crystallization.

	BVD 52-A	Cumulate	Composition of minerals				Calculated liquid (C _L) ¹	ED 1 (C _L) ²
	(C ₀) ³	(C _s)	Pl ^c	Cpx ^c	Opx ^c	Amp ^c		Trondhjemite ^b
	Tonalite ^b	Bulk	71.43%	21.46%	4.55%	2.56%		
Major elements (wt.%)								
SiO ₂	69.75	59.62	61.42	53.06	51.93	49.45	78.26	78.39
TiO ₂	0.76	0.05	0.00	0.08	0.07	0.92	0.82	0.18
Al ₂ O ₃	13.85	17.04	23.21	0.44	0.18	5.80	11.30	11.44
FeO*	2.71	3.84	0.05	9.78	28.86	13.66	1.76	1.74
MnO	0.03	0.08	0.00	0.15	0.90	0.24	0.00	0.01
MgO	1.76	3.88	0.00	12.54	16.93	14.29	0.28	0.61
CaO	5.30	8.81	5.17	21.89	0.49	11.16	2.41	2.44
Na ₂ O	5.35	6.40	8.59	0.70	0.05	1.17	4.54	4.61
K ₂ O	0.49	0.28	0.36	0.02	0.00	0.63	0.63	0.58
Trace elements (ppm)								
Ba	250.0						196.9	191.5
Rb	9.0						12.4	8.4
Sr	317.0						288.8	291.0
Y	16.5						27.5	30.0
Zr	324.0						378.6	307.0
Nb	12.0						15.3	14.4
La	14.40						10.56	8.00
Ce	23.10						21.71	19.00
Nd	10.20						13.05	13.10
Sm	2.91						3.64	3.43
Eu	0.95						1.23	1.25
Gd	3.29						4.39	4.35
Yb	1.74						3.08	3.44
Lu	0.330						0.580	0.640

ΣR²=0.565.

FC=45%.

ΣR²: Sum of the squared residuals; FC: Fractional crystallization. All iron is reported as FeO; ^aBulk composition from Marangoanha *et al.* (2019a); ^bOriginal oxide values recast to 100%; ^cMineral composition values from this work.**Table 6.** Summary of crystallization parameter data for selected charnockitic rocks (*lato sensu*) from Carajás Province and worldwide terranes.

Unit	T (°C)	P (MPa)	fO ₂	H ₂ O _{met} (wt.%)
Carajás Province (Amazonian craton, Brazil)				
Café enderbite ¹	1,150-850	750-600	Oxidized: FMQ to NNO + 1.7	4.8-5.6
Opx-granodiorites from Ourilândia do Norte ²	1,061-833	310-190	Oxidized: > NNO	> 4
Worldwide terranes				
Louis Lake batholith (Wyoming Province, USA) ³	~800	700-500	Oxidized: FMQ+1.5 to 1.8	2-4
Charnockites from Leaf River suite (Canada) ⁴	1,100-800	600-400	Oxidized: FMQ+0.6 to 2	< 2
Matok pluton (Limpopo Belt, South Africa) ⁵	900-800	860-330	Oxidized: > NNO	> 5
Charnockite massifs from southern India ^{6*}	1,036-679	900-600	<i>n.d.</i>	<i>n.d.</i>
Luyashan charnockite (North China craton) ⁷	1,000-900	<i>n.d.</i>	<i>n.d.</i>	<3

n.d.: not determined; References: ¹This work, ²Félix *et al.* (2020), ³Frost *et al.* (2000), ⁴Percival and Mortensen (2002), ⁵Rapopo (2011), ⁶Rajesh and Santosh (2004), ⁷Yang and Santosh (2015); *Composed of the Pallavaram, Shevroy Hill, Biligirirangan Hill, Nilgiri Hill, northern Kerala, Cardamom Hill, and Nagercoil massifs.

Concerning H_2O_{melt} , the stability of orthopyroxene is also controlled by low water content in the charnockitic magma (Santosh and Yoshikura 2001). In fact, over the years, most authors have emphasized the ‘water-poor melt condition’ as a determinant for orthopyroxene to become stable in the melt (Clemens and Wall 1981, Frost and Frost 2008, and references therein). The rocks from the Café enderbite show H_2O_{melt} contents of 4.8–5.6 wt.%, and some other occurrences, such as opx-bearing granodiorites from the Ourilândia do Norte region and Matok pluton, present similar values, while the Louis Lake batholith, Leaf River suite, and Luyashan charnockite display lower water contents, generally < 4 wt.% (cf. Tab. 6). However, the H_2O_{melt} values recorded by the studied enderbite are in accordance with Percival and Mortensen’s (2002) findings. These authors show through a schematic T versus H_2O_{melt} diagram based on Naney’s (1983) experimental results for calc-alkaline felsic melts that the stability field of orthopyroxene can be reached between ~ 4 and 6 wt.% water content in the magma, under conditions of $\sim 1,000$ – 800°C and 500 MPa (this pressure is obtained through a linear interpolation between the wide pressure range of 800 – 200 MPa). Therefore, these conditions entirely cover those found in the rocks from the Café enderbite, with an emphasis on the water content in the magma. Nevertheless, other parameters should be considered to account for orthopyroxene stability even in magmas that are less water undersaturated, as a free CO_2 -rich fluid phase coexisting with the magma during its evolution producing an effective dilution of H_2O in the melt and hence favor orthopyroxene stabilization/crystallization (Frost and Frost 1987, Ridley 1992). Although the present work does not address the CO_2 content in the rocks from the Café enderbite, fluid inclusion studies from Wilmart *et al.* (1991), Frost *et al.* (2000), and Harlov *et al.* (2013) reveal that volatiles in metaluminous igneous charnockites are CO_2 -rich, therefore stabilizing orthopyroxene at low, near-solidus temperatures (the Café enderbite is strongly metaluminous; Marangoanha *et al.* 2019a).

This brief approach shows remarkable similarities between the Café enderbite and the selected Archean–Proterozoic igneous charnockite occurrences around the world in terms of intrinsic crystallization parameters (T – P – fO_2 – H_2O_{melt}), regardless of the specific geologic setting of each case.

Implications for the genesis of the Neoproterozoic Café enderbite

The ~ 2.74 Ga Café enderbite plutons are located in the Canaã dos Carajás domain, central portion of Carajás Province (cf. Fig. 1). In general, this portion of the crust evolved after Mesoproterozoic and Neoproterozoic events, marked by magmatism, metamorphism, hydrothermalism, and deformation episodes (Pidgeon *et al.* 2000, Moreto *et al.* 2011, Feio *et al.* 2012, 2013, Cunha *et al.* 2016, Oliveira *et al.* 2018, Marangoanha *et al.* 2019a, 2019b, 2020, Silva *et al.* 2021). A detailed study from Marangoanha *et al.* (2019a) identified three specific Archean events responsible for the Canaã dos Carajás domain formation and cratonization as follows:

- from 3.05 to 2.93 Ga, TTG crust was generated in a subduction setting;

- from 2.89 to 2.84 Ga, large volumes of anatectic granites were formed in a collisional setting, accompanied by crustal thickening and granulitic metamorphism in the TTG crust;
- in the Neoproterozoic, from 2.75 to 2.73 Ga, the lowermost mafic crust was delaminated during crustal thickening.

Concerning the geological setting, Marangoanha *et al.* (2019a) stated that the formation of Neoproterozoic granitoids in this portion of the crust — which include the Café enderbite — was triggered by delamination process at 2.75–2.73 Ga. More specifically, the lowermost mafic crust was delaminated during crustal thickening, causing crustal underplating by mantle-derived mafic magma followed by partial melting of mafic granulite (lower continental crust), which was responsible for the origin of the parental liquid of the Café enderbite. Geochemical modeling performed by these authors yielded a quartz dioritic liquid through 21% partial melting of a mafic granulite. Additionally, this study shows, through geochemical modeling, that the rocks from the Café enderbite evolved by fractional crystallization with a very high crystal content. According to this modeling, two fractional crystallization stages were proposed. First, the initial liquid, with quartz dioritic composition (formed by partial melting of the mafic granulite; Marangoanha *et al.* 2019a), evolved by 92% fractional crystallization to form an orthopyroxene-bearing tonalite (cf. Fig. 11A; Tab. 4). Then, this freshly formed tonalitic liquid evolved by 45% fractional crystallization to form an orthopyroxene-bearing trondhjemite (cf. Fig. 11B; Tab. 5). A recent experimental study by Zhao *et al.* (2018) in the Jiuzhou pluton (South China) demonstrated that in charnockitic igneous systems, orthopyroxene is preserved only in solidification zones in which it formed early in a magmatic system with a high crystal content of $\geq 40\%$. These authors argued that such a high crystal content leaves a relatively small proportion of melt for reaction with orthopyroxene, hence increasing the ‘survival chances’ of this mineral. On the other hand, according to these authors, at low crystal content ($< 40\%$), orthopyroxene that is formed early should be totally resorbed. However, Zhao *et al.* (2018) highlighted that other factors must also be considered to make orthopyroxene stable in igneous charnockites, such as magma composition, low water activity (aH_2O), and high temperature, pressure, and CO_2 , which all represent deep crustal conditions (Janardhan *et al.* 1982, Frost *et al.* 2000, Grantham *et al.* 2012).

Although the first stage of fractional crystallization (quartz diorite \rightarrow opx-tonalite) points to formation of an extremely high crystal content of 92% (cf. Fig. 11A; Tab. 4), we believe that this value is somewhat overestimated and does not give a reliable geological scenario. However, the Sr versus Ba diagram in Fig. 11C shows that the same fractionating assemblage proportion and initial and daughter liquid compositions (samples BVD 35-A and BVD 52-A, respectively) yield a model with generation of $\sim 60\%$ crystal content, which represents a value in accordance with Zhao *et al.*’s (2018) experiments.

In addition to the fractionation of a high crystal content advocated by Zhao *et al.* (2018), other proposals can be

considered related to orthopyroxene stability in igneous charnockites. Frost *et al.* (1989) showed that charnockitic plutons represent cumulates that formed early in the crystallization of a pluton and that were isolated from later, more hydrous portions of the batholith. Extending this idea to the studied enderbites, Santos *et al.* (2013) identified cumulate rocks (composed of Opx + Cpx + Pl ± Amp) spatially associated with the Pium diopside-norite, which also crops out close to the Café enderbite plutons (cf. Fig. 2). Marangoanha *et al.* (2020) suggested, based on geochemical modeling, geochronology, and Hf–Nd isotopes, that the Pium diopside-norite has no cogenetic link with the Café enderbite, whereas the two units are coeval and geographically associated. Hence, these cumulate occurrences mapped by Santos *et al.* (2013) could potentially represent the cumulate counterpart of the Café enderbite since these authors do not clarify the real significance or links of these particular rocks (cumulates) in the Pium diopside-norite.

All the considerations raised to this point indicate that the Café enderbite potentially involved the main proposals related to igneous charnockite origin in the literature, listed by Rajesh (2007):

- *Partial melt from mafic lower crustal granulite* (Duchesne *et al.* 1989, Emslie *et al.* 1994, Longhi *et al.* 1999, Rajesh and Santosh 2004, Rajesh 2007): As proposed by Marangoanha *et al.* (2019a), the least evolved rocks from the Café enderbite, represented by the quartz diorites, formed by 21% partial melt of a Mesoproterozoic mafic granulite associated with delamination;
- *Extensive fractional crystallizations of ferrodiorites* (Vander Auwera *et al.* 1998, Scoates and Lindsley 2000). If we consider our initial liquid, formed by partial melting of mafic granulite, to be ferrodiorite (according to Fig. 1 from Frost and Frost 2008), this statement is absolutely true, as demonstrated by our fractional crystallization models based on the high crystal content (45–60%) (Figs. 11A–11C; Tabs. 4 and 5);
- *Residues or cumulates after the removal of an evolved (granitic) melt* (Emslie 1991, Mitchell *et al.* 1996, Markl and Höhndorf 2003). Although this process was not tested in the present work, it was not in fact rejected due to the cumulate occurrences mapped by Santos *et al.* (2013). Furthermore, as this portion of Carajás Province is marked by intense ~2.74 Ga magmatism, a possible pyroxene-free granitic counterpart (similar to the Vila Jussara suite; see Section “Charnockitic Magmatism of Carajás Province”) is not totally eliminated, and this process could have played a discrete role.

In summary, the Café enderbite quite clearly evolved under a complex scenario that encompassed more than a simple petrogenetic process, as established for most igneous charnockites worldwide. The processes involved in the generation of the Café enderbite are partial melting of a mafic granulite (lower crust) followed by a minimum of two fractional crystallization stages with high crystal content (45–60%) under crystallization conditions of 1,150–850°C and 750–600 MPa, high oxygen fugacity (FMQ to NNO + 1.7 buffers) and moderate H_2O_{melt} (4.8–5.6 wt.%). All these particular conditions were assisted

by a N–S pure shear-dominated transpressional regime, with an E–W sinistral sense of tectonic movement responsible for the syntectonic character printed on these charnockitic granitoids at 2.75–2.73 Ga (Oliveira *et al.* 2018, Marangoanha *et al.* 2019a, 2019b, 2020).

CONCLUSIONS

- The granitoids from the Neoproterozoic Café enderbite are composed of orthopyroxene-bearing tonalites and trondhjemites, with subordinate quartz diorite, reflecting a wide range of silica contents (53–80 wt.%). This broad SiO_2 range argues against a simple partial melting process from a mafic source. Geochemical modeling shows that two stages of fractional crystallization (stage 1: quartz diorite→opx-tonalite; stage 2: opx-tonalite→opx-trondhjemite) were the likely petrogenetic processes responsible for the Café enderbite evolution;
- Separation of a high crystal content during fractional crystallization of the studied charnockites, between 45 and 60% (or even higher), was the key factor that preserved orthopyroxene in the magmatic system, since this degree of fractionation allows a relatively small proportion of melt to react with the early-formed orthopyroxene;
- Constrained intrinsic parameters show that the Café enderbite evolved under high temperature and pressure conditions of 1,150–850°C and 750–600 MPa, respectively, with moderate water contents in the melt (4.8–5.6 wt.%) and under relatively oxidizing conditions, buffered between FMQ and NNO + 1.7;
- The constrained T–P– fO_2 – H_2O_{melt} parameters from the studied rocks are quite similar to those from Precambrian magmatic charnockites *lato sensu* worldwide, confirming that, in addition to some specific peculiarities (probably promoted by their particular geological setting), they present ‘standard crystallization conditions’, which require high T, P, and CO_2 , low H_2O_{melt} and a broad range of fO_2 ; these conditions characterize deep crustal settings.

ACKNOWLEDGMENTS

The authors would like to acknowledge the Laboratório de Microanálises staff from the Universidade Federal do Pará (UFPA) for assistance with the electron microprobe mineral chemical analyses. B.M. thanks the Programa Nacional de Pós-Doutorado — Coordenação de Aperfeiçoamento de Pessoal de Nível Superior (PNPD/CAPES) for a postdoctoral scholarship (Proc. 88887.363462/2019-00). This research received financial support from the Conselho Nacional de Desenvolvimento Científico e Tecnológico (CNPq) (D.C. Oliveira; Proc. 435552/2018-0 and 311647/2019-7) and Pró-Reitoria de Pesquisa e Pós-Graduação — Programa de Apoio à Publicação Qualificada (PROPESP/PAPQ/UFPA; Edital 06/2021 — Proc. 23073.011949/2021-10). Constructive criticism from the reviewers P. Alasino and J. Mendes substantially improved the quality of this article. C. Grohmann and R.J. Pankhurst are acknowledged for their careful editorial handling and constructive comments.

ARTICLE INFORMATION

Manuscript ID: 20210092. Received on: 31 DEC 2021. Approved on: 16 MAY 2022.

How to cite this article: Marangoanha B., Oliveira D.C., Lamarão C.N., Marques G.T., Silva L.R. Geothermobarometry and geochemical modeling of Archean charnockites from Carajás Province, Amazonian craton (Brazil). *Brazilian Journal of Geology*, 52(4):e20210092. <https://doi.org/10.1590/2317-488920220210092>

B.M.: writing — original draft preparation, conceptualization, methodology, and investigation; D.C.O.: writing — review and editing, supervision, and funding acquisition; C.N.L. methodology; G.T.M.: methodology; L.R.S.: writing — review and editing and conceptualization.

Competing interests: the authors declare that they have no known competing financial interests or personal relationships that could have appeared to influence the work reported in this article.

REFERENCES

- Almeida J.A.C., Dall'Agnol R., Dias S.B., Althoff F.J. 2010. Origin of the Archean leucogranodiorite–granite suites: Evidence from the Rio Maria terrane and implications for granite magmatism in the Archean. *Lithos*, **120**(3-4):235-257. <https://doi.org/10.1016/j.lithos.2010.07.026>
- Almeida J.A.C., Dall'Agnol R., Oliveira M.A., Macambira M.J.B., Pimentel M.M., Râmô O.T., Guimarães F.V., Leite A.A.S. 2011. Zircon geochronology and geochemistry of the TTG suites of the Rio Maria granite-greenstone terrane: Implications for the growth of the Archean crust of Carajás Province, Brazil. *Precambrian Research*, **187**(1-2):201-221. <https://doi.org/10.1016/j.precamres.2011.03.004>
- Althoff F.J., Barbey P., Boullier A.M. 2000. 2.8-3.0 Ga plutonism and deformation in the SE Amazonian craton: the Archean granitoids of Marajoara (Carajás Mineral Province, Brazil). *Precambrian Research*, **104**(1-4):187-206. [https://doi.org/10.1016/S0301-9268\(00\)00103-0](https://doi.org/10.1016/S0301-9268(00)00103-0)
- Anderson J.L., Barth A.P., Wooden J.L., Mazdab F. 2008. Thermometers and thermobarometers in granitic systems. *Reviews in Mineralogy and Geochemistry*, **69**(1):121-142. <https://doi.org/10.2138/rmg.2008.69.4>
- Anderson J.L., Smith D.R. 1995. The effects of temperature and fO₂ on the Al-in-hornblende barometer. *American Mineralogist*, **80**(5-6):549-559. <https://doi.org/10.2138/am-1995-5-614>
- Avelar V.G., Lafon J.M., Correia Jr. F.C., Macambira E.M.B. 1999. O Magmatismo arqueano da região de Tucumã – Província Mineral de Carajás: Novos resultados geocronológicos. *Revista Brasileira de Geociências*, **29**(4):454-460. <https://doi.org/10.25249/0375-7536.1999294453460>
- Barros C.E.M., Sardinha A.S., Barbosa J.P.O., Macambira M.J.B. 2009. Structure, petrology, geochemistry and zircon U-Pb and Pb-Pb geochronology of the synkinematic Archean (2.7 Ga) A-type granites from the Carajás Metallogenic Province, northern Brazil. *Canadian Mineralogist*, **47**:1423-1440.
- Best M.G., Christiansen E.H. 2001. *Igneous petrology*. Massachusetts: Blackwell Science, 458 p.
- Bogaerts M., Scaillet B., Vander Auwera J. 2006. Phase equilibria of the Lyngdal granodiorite (Norway): Implications for the origin of metaluminous ferroan granitoids. *Journal of Petrology*, **47**(12):2405-2431. <https://doi.org/10.1093/petrology/egl049>
- Bowden P., Batchelor R.A., Chappell B.W., Didier J., Lameyre J. 1984. Petrological, geochemical and source criteria for the classification of granitic rocks: A discussion. *Physics of the Earth and Planetary Interiors*, **35**(1-3):1-11. [https://doi.org/10.1016/0031-9201\(84\)90029-3](https://doi.org/10.1016/0031-9201(84)90029-3)
- Brown M. 1994. The generation, segregation, ascent and emplacement of granite magma: the migmatite-to-crustally-derived granite connection in thickened orogens. *Earth Science Reviews*, **36**(1-2):83-130. [https://doi.org/10.1016/0012-8252\(94\)90009-4](https://doi.org/10.1016/0012-8252(94)90009-4)
- Brown M. 2004. The mechanism of melt extraction from lower continental crust of orogens. *Earth and Environmental Science Transactions of the Royal Society of Edinburgh*, **95**(1-2):35-48. <https://doi.org/10.1017/S0263593300000900>
- Brown M. 2007. Crustal melting and melt extraction, ascent and emplacement in orogens: Mechanisms and consequences. *Journal of the Geological Society of London*, **164**(4):709-730. <https://doi.org/10.1144/0016-76492006-171>
- Bucher K., Frost B.R. 2006. Fluid transfer in high-grade metamorphic terrains intruded by anorogenic granites: The Thor Range, Antarctica. *Journal of Petrology*, **47**(3):567-593. <https://doi.org/10.1093/petrology/egi086>
- Clemens J.D., Wall V.J. 1981. Origin and crystallization of some peraluminous (S-type) granitic magmas. *The Canadian Mineralogist*, **19**(1):111-132.
- Cunha I.R.V., Dall'Agnol R., Feio G.R.L. 2016. Mineral chemistry and magnetic petrology of the Archean Planalto Suite, Carajás Province – Amazonian Craton: Implications for the evolution of ferroan Archean granites. *Journal of South American Earth Sciences*, **67**:100-121. <https://doi.org/10.1016/j.jsames.2016.01.007>
- Dall'Agnol R., Cunha I.R.V., Guimarães F.V., Oliveira D.C., Teixeira M.F.B., Feio G.R.L., Lamarão C.N. 2017. Mineralogy, geochemistry, and petrology of Neoproterozoic ferroan to magnesian granites of Carajás Province, Amazonian Craton: The origin of hydrated granites associated with charnockites. *Lithos*, **277**:3-32. <https://doi.org/10.1016/j.lithos.2016.09.032>
- Dall'Agnol R., Oliveira D.C., Guimarães F.V., Gabriel E.O., Feio G.R.L., Lamarão C.N., Althoff F.J., Santos P.A., Teixeira M.F.B., Silva A.C., Rodrigues D.S., Santos M.J.P., Silva C.R.P., Santos R.D., Santos P.J.L. 2013. Geologia do Subdomínio de Transição do Domínio Carajás – Implicações para a evolução arqueana da Província Carajás - Pará. In: Simpósio de Geologia da Amazônia, 13., Belém. *Short Papers...* CD-ROM.
- Dall'Agnol R., Oliveira M.A., Almeida J.A.C., Althoff F.J., Leite A.A.S., Oliveira D.C., Barros C.E.M. 2006. Archean and Paleoproterozoic granitoids of the Carajás metallogenic province, eastern Amazonian craton. In: Dall'Agnol R., Rosa-Costa L.T., Klein E.L. (eds.). *Symposium on magmatism: crustal evolution, and metallogenesis of the Amazonian Craton*. Abstracts Volume and Field Trips Guide. Belém: PRONEX-UFPA/SBG-NO, p. 99-150.
- Dall'Agnol R., Râmô O.T., Magalhães M.S., Macambira M.J.B. 1999. Petrology of the anorogenic, oxidized Jamon and Musa granites, Amazonian Craton: Implications for the genesis of Proterozoic, A-type granites. *Lithos*, **46**(3):431-462. [https://doi.org/10.1016/S0024-4937\(98\)00077-2](https://doi.org/10.1016/S0024-4937(98)00077-2)
- Dall'Agnol R., Teixeira N.P., Râmô O.T., Moura C.A.V., Macambira M.J.B., Oliveira D.C. 2005. Petrogenesis of the Paleoproterozoic, rapakivi, A-type granites of the Archean Carajás Metallogenic Province, Brazil. *Lithos*, **80**(1-4):101-129. <https://doi.org/10.1016/j.lithos.2004.03.058>
- Deer W.A., Howie A., Sussman J. 1986. *An introduction to rock-forming minerals*. Hertfordshire: Longman, 528 p.
- Deer W.A., Howie R.A., Zussman M.A. 1992. *An introduction to the rock-forming minerals*. 2nd ed. New York: Prentice Hall, 696 p.
- DePaolo D.J. 1981. Trace element and isotopic effects of combined wallrock assimilation and fractional crystallization. *Earth and Planetary Science Letters*, **53**(2):189-202. [https://doi.org/10.1016/0012-821X\(81\)90153-9](https://doi.org/10.1016/0012-821X(81)90153-9)
- Duchesne J.C., Wilmart E., DemaiFFE D., Hertogen J. 1989. Monzonorites from Rogaland southwest Norway: A series of rocks coeval but not comagmatic with massif-type anorthosites. *Precambrian Research*, **45**(1-3):111-128. [https://doi.org/10.1016/0301-9268\(89\)90034-X](https://doi.org/10.1016/0301-9268(89)90034-X)
- Emslie R.F. 1991. Granitoids of rapakivi granite-anorthosite and related associations. *Precambrian Research*, **51**(1-4):173-192. [https://doi.org/10.1016/0301-9268\(91\)90100-0](https://doi.org/10.1016/0301-9268(91)90100-0)
- Emslie R.F., Hamilton M.A., Thierault R.J. 1994. Petrogenesis of a Mid-Proterozoic Anorthosite-Mangerite-Charnockite-Granite (AMCG) complex: Isotopic and chemical evidence from the Nain plutonic suite. *The Journal of Geology*, **102**(5):539-558. <https://doi.org/10.1086/629697>

- Ersoy E.Y. 2013. PETROMODELER (Petrological Modeler): A Microsoft Excel spreadsheet program for modelling melting, mixing, crystallization and assimilation processes in magmatic systems. *Turkish Journal of Earth Sciences*, **22**(1):115-125. <https://doi.org/10.3906/yer-1104-6>
- Fegley B. 2013. *Practical chemical thermodynamics for geoscientists*. London: Elsevier, 732 p.
- Feio G.R.L., Dall'Agnol R., Dantas E.L., Macambira M.J.B., Gomes A.C.B., Sardinha A.S., Oliveira D.C., Santos R.D., Santos P.A. 2012. Geochemistry, geochronology and origin of the Neoproterozoic Planalto granite suite, Carajás, Amazonian craton: A-type or hydrated charnockitic granites? *Lithos*, **151**:57-73. <https://doi.org/10.1016/j.lithos.2012.02.020>
- Feio G.R.L., Dall'Agnol R., Dantas E.L., Macambira M.J.B., Santos J.O.S., Althoff F.J., Soares J.E.B. 2013. Archean granitoid magmatism in the Canaã dos Carajás area: Implications for crustal evolution of the Carajás province, Amazonian craton, Brazil. *Precambrian Research*, **227**:157-185. <https://doi.org/10.1016/j.precamres.2012.04.007>
- Félix W.Q., Oliveira D.C., Silva L.R., Silva F.F. 2020. Charnockites from Carajás Province, SE Amazonian Craton (Brazil): Petrogenetic constraints and intensive crystallization parameters. *Journal of South American Earth Sciences*, **101**:102598. <https://doi.org/10.1016/j.jsames.2020.102598>
- Foster M.D. 1960. Interpretation of composition of trioctahedral micas. U.S. *Geological Survey Professional Paper*, **354**(B):11-49. <https://doi.org/10.3133/PP354B>
- Frost B.R., Frost C.D. 1987. CO₂ melts and granulite metamorphism. *Nature*, **327**:503-506. <https://doi.org/10.1038/327503a0>
- Frost B.R., Frost C.D. 2008. On charnockites. *Gondwana Research*, **13**(1):30-44. <https://doi.org/10.1016/j.gr.2007.07.006>
- Frost B.R., Frost C.D., Hulsebosch T.P., Swapp S.M. 2000. Origin of the charnockites of the Louis Lake Batholith, Wind River Range, Wyoming. *Journal of Petrology*, **41**(12):1759-1776. <https://doi.org/10.1093/petrology/41.12.1759>
- Frost B.R., Frost C.D., Touret J.L.R. 1989. Magmas as a source of heat and fluids in granulite metamorphism. In: Bridgwater D. (ed.). *Fluid movements: element transport and the composition of the deep crust*. NATO ASI series, 281. Dordrecht: Springer, p. 1-18. https://doi.org/10.1007/978-94-009-0991-5_1
- Frost C.D., Frost B.R., Chamberlain K.R., Edwards B.R. 1999. Petrogenesis of the 1.43 Ga Sherman batholith, SE Wyoming: A reduced rapakivi-type anorogenic granite. *Journal of Petrology*, **40**(12):1771-1802. <https://doi.org/10.1093/petrology/40.12.1771>
- Fuhrman M.L., Frost B.R., Lindsley D.H. 1988. The petrology of the Sybille Monzosyenite, Laramie Anorthosite Complex, Wyoming. *Journal of Petrology*, **29**(3):699-729. <https://doi.org/10.1093/petrology/29.3.699>
- Gabriel E.O., Oliveira D.C. 2014. Geologia, petrografia e geoquímica dos granitoides arqueanos de alto magnésio da região de Água Azul do Norte, porção sul do Domínio Carajás, Pará. *Boletim do Museu Paraense Emílio Goeldi, Ciências Naturais*, **9**(3):533-564. <https://doi.org/10.46357/bcnaturais.v9i3.509>
- Grantham G.H., Mendonidis P., Thomas R.J., Satish-Kumar M. 2012. Multiple origins of charnockite in the Mesoproterozoic Natal belt, KwaZulu-Natal, South Africa. *Geoscience Frontiers*, **3**(6):755-771. <https://doi.org/10.1016/j.gsf.2012.05.006>
- Guimarães F.V.G., Dall'Agnol R., Almeida J.A.C., Oliveira M.A. 2010. Caracterização geológica, petrográfica e geoquímica do Trondhjemito Mogno e Tonalito Mariázinha, Terreno Granito-Greenstone de Rio Maria - Pará. *Revista Brasileira de Geociências*, **40**(2):196-211. <https://doi.org/10.25249/0375-7536.2010402196211>
- Hammarstrom J.M., Zen E. 1986. Aluminum in hornblende: An empirical igneous geobarometer. *American Mineralogist*, **71**(11-12):1297-1313.
- Hanson G.N. 1978. The application of trace elements to the petrogenesis of igneous rocks of granitic composition. *Earth Planetary Sciences Letters*, **38**(1):26-43. [https://doi.org/10.1016/0012-821X\(78\)90124-3](https://doi.org/10.1016/0012-821X(78)90124-3)
- Hanson G.N. 1989. An approach to trace element modeling using a simple igneous system as an example. In: Lipin B.R., McKay G.A. (eds.). *Geochemistry and mineralogy of rare earth elements. Reviews in Mineralogy*, 21. Berlin-Boston: De Gruyter, p. 79-98. <https://doi.org/10.1515/9781501509032-007>
- Harlov D.E., Van Den Kerkhof A., Johansson L. 2013. The Varberg-Torpa charnockite-granite association, SW Sweden: Mineralogy, petrology, and fluid inclusion chemistry. *Journal of Petrology*, **54**(1):3-40. <https://doi.org/10.1093/petrology/egs060>
- Harrison T.M., Watson E.B. 1984. The behavior of apatite during crustal anatexis: Equilibrium and kinetic considerations. *Geochimica et Cosmochimica Acta*, **48**(7):1467-1477. [https://doi.org/10.1016/0016-7037\(84\)90403-4](https://doi.org/10.1016/0016-7037(84)90403-4)
- Henry D., Guidotti C., Thomson J. 2005. The Ti-saturation surface for low- to medium pressure metapelitic biotites: Implications for geothermometry and Ti-substitution mechanism. *American Mineralogist*, **90**(2-3):316-328. <https://doi.org/10.2138/am.2005.1498>
- Holdsworth R.E., Pinheiro R.V.L. 2000. The anatomy of shallow-crustal transpressional structures: Insights from the Archaean Carajás fault zone, Amazon, Brazil. *Journal of Structural Geology*, **22**(8):1105-1123. [https://doi.org/10.1016/S0191-8141\(00\)00036-5](https://doi.org/10.1016/S0191-8141(00)00036-5)
- Holland T.H. 1900. The charnockite series, a group of Archean hypersthene rocks in Peninsular India. *Memoirs of the Geological Survey of India*, **28**:192-249.
- Holland T.H., Blundy J. 1994. Non-ideal interactions in calcic amphiboles and their bearing on amphibole-plagioclase thermometry. *Contributions to Mineralogy and Petrology*, **116**:433-447. <https://doi.org/10.1007/BF00310910>
- Hollister L.S., Grissom G.C., Peters E.K., Stowell H.H., Sisson V.B. 1987. Confirmation of the empirical correlation of Al in hornblende with pressure of solidification of calc-alkaline plutons. *American Mineralogist*, **72**(3-4):231-239.
- Hossain I., Tsunogae T. 2014. Crystallization conditions and petrogenesis of the Paleoproterozoic basement rocks in Bangladesh: An evaluation of biotite and coexisting amphibole mineral chemistry. *Journal of Earth Science*, **25**(1):87-97. <https://doi.org/10.1007/s12583-014-0402-1>
- Icenhower J.P., Dymek R.F., Weaver B.L. 1998. Evidence for an enriched mantle source for jotunite (orthopyroxene monzodiorite) associated with the St. Urbain anorthosite, Quebec. *Lithos*, **42**(3-4):191-212. [https://doi.org/10.1016/S0024-4937\(97\)00042-X](https://doi.org/10.1016/S0024-4937(97)00042-X)
- Ishihara S. 1981. The granitoid series and mineralization. *Economic Geology*, **75**:458-484. <https://doi.org/10.5382/AV75.14>
- Janardhan A.S., Newton R.C., Hansen E.C. 1982. The transformation of amphibolite facies gneiss to charnockite in southern Karnataka and northern Tamil Nadu, India. *Contributions to Mineralogy and Petrology*, **79**:130-149. <https://doi.org/10.1007/BF01132883>
- Janoušek V., Farrow C.M., Erban V. 2003. GCDKit: New PC software for interpretation of whole-rock geochemical data from igneous rocks. *Geochimica et Cosmochimica Acta*, **67**(18):A186.
- Johnson M.C., Rutherford M.J. 1989. Experimental calibration of the aluminum-in-hornblende geobarometer with application of Long Valley caldera (California) volcanic rocks. *Geology*, **17**(9):837-841. [https://doi.org/10.1130/0091-7613\(1989\)017<0837:ECOTAI>2.3.CO;2](https://doi.org/10.1130/0091-7613(1989)017<0837:ECOTAI>2.3.CO;2)
- Klimm K., Holtz F., Johannes W., King P.L. 2003. Fractionation of metaluminous A-type granites: An experimental study of the Wangrah suite, Lachlan Fold Belt, Australia. *Precambrian Research*, **124**(2-4):327-341. [https://doi.org/10.1016/S0301-9268\(03\)00092-5](https://doi.org/10.1016/S0301-9268(03)00092-5)
- Kolker A., Lindsley D.H. 1989. Geochemical evolution of the Maloin Ranch pluton, Laramie Anorthosite Complex, Wyoming, petrology and mixing relations. *American Mineralogist*, **74**(3-4):307-324.
- Kriegsman L. 2001. Partial melting, partial melt extraction and partial back reaction in anatectic migmatites. *Lithos*, **56**(1):75-96. [https://doi.org/10.1016/S0024-4937\(00\)00060-8](https://doi.org/10.1016/S0024-4937(00)00060-8)
- Lameyre J., Bowden P. 1982. Plutonic rock type series: Discriminations of various granitoid series and related rocks. *Journal of Volcanology and Geothermal Research*, **14**(1-2):169-186. [https://doi.org/10.1016/0377-0273\(82\)90047-6](https://doi.org/10.1016/0377-0273(82)90047-6)
- Le Maître R.W., Streckeis A., Zanettin B., Le Bas M.J., Bonin B., Bateman P., Bellieni G., Dudek A., Efremova J., Keller J., Lameyre J., Sabine P.A., Schmidt R., Sørensen H., Woolley A.R. 2002. Igneous rocks. A classification and glossary of terms. In: Recommendations of the International Union of Geological Sciences Subcommission on the Systematics of Igneous Rocks. Cambridge: Cambridge University Press, 252 p.

- Leake B.E., Wooley A.R., Arps C.E.S., Birch W.D., Gilbert M.C., Grice J.D., Hawthorne F.C., Kato A., Kisch H.J., Krivovichev V.G., Linthout K., Laird J., Mandarino J.A., Maresch W.V., Nickel E.H., Schumacher J., Smith J.C., Stephenson N.C.N., Ungaretti L., Whittaker E.J.W., Youzhi G. 1997. Nomenclature of amphiboles: Report of the subcommittee on amphiboles of the international mineralogical association commission on new minerals and Mineral names. *Mineralogical Magazine*, **61**(2):295-321.
- Leite A.A.S., Dall'Agnol R., Macambira M.J.B., Althoff F.J. 2004. Geologia e geocronologia dos granitóides arqueanos da região de Xinguaçu (PA) e suas implicações na evolução do Terreno Granito-Greenstone de Rio Maria. *Revista Brasileira de Geociências*, **34**(4):447-458. <https://doi.org/10.25249/0375-7536.2004344447458>
- Li W., Cheng Y., Yang Z. 2019. Geo-fO2: Integrated software for analysis of magmatic oxygen fugacity. *Geochemistry, Geophysics, Geosystems*, **20**(5):2542-2555. <https://doi.org/10.1029/2019GC008273>
- Longhi J., Vander Auwera J., Fram M.S., Duchesne J.C. 1999. Some phase equilibrium constraints on the origin of Proterozoic (massif) anorthositic and related rocks. *Journal of Petrology*, **40**(2):339-362. <https://doi.org/10.1093/ptro/40.2.339>
- Luhr J.F., Carmichael I.S.E., Varekamp J. 1984. The 1982 eruptions of El Chichón Volcano, Chiapas, Mexico: Mineralogy and petrology of the anhydrite-bearing pumices. *Journal of Volcanology and Geothermal Research*, **23**(1-2):69-108. [https://doi.org/10.1016/0377-0273\(84\)90057-X](https://doi.org/10.1016/0377-0273(84)90057-X)
- Machado N., Lindenmayer Z.G., Krogh T.E., Lindenmayer D. 1991. U-Pb geochronology of Archean magmatism and basement reactivation in the Carajás area, Amazon shield, Brazil. *Precambrian Research*, **49**(3-4):329-354. [https://doi.org/10.1016/0301-9268\(91\)90040-H](https://doi.org/10.1016/0301-9268(91)90040-H)
- Marangoanha B., Oliveira D.C., Dall'Agnol R. 2019a. The Archean granulite-enderbite complex of the northern Carajás province, Amazonian craton (Brazil): Origin and implications for crustal growth and cratonization. *Lithos*, **350-351**:105275. <https://doi.org/10.1016/j.lithos.2019.105275>
- Marangoanha B., Oliveira D.C., Galarza M.A., Marques G.T. 2020. Crustal anatexis and mantle-derived magmas forming Neoproterozoic A-type granitoids in Carajás Province, northern Brazil: Petrological evidence and tectonic control. *Precambrian Research*, **338**:105585. <https://doi.org/10.1016/j.precamres.2019.105585>
- Marangoanha B., Oliveira D.C., Oliveira V.E.S., Galarza M.A., Lamarão C.N. 2019b. Neoproterozoic A-type granitoids from Carajás province (Brazil): New insights from geochemistry, geochronology and microstructural analysis. *Precambrian Research*, **324**:86-108. <https://doi.org/10.1016/j.precamres.2019.01.010>
- Markl G., Höhndorf A. 2003. Isotopic constraints on the origin of AMCG-suite rocks on the Lofoten Islands, N Norway. *Mineralogy and Petrology*, **78**:149-171. <https://doi.org/10.1007/s00710-002-0229-9>
- McDonough W.F., Sun S.S. 1995. The composition of the Earth. *Chemical Geology*, **120**(3-4):223-253. [https://doi.org/10.1016/0009-2541\(94\)00140-4](https://doi.org/10.1016/0009-2541(94)00140-4)
- Melo G.H.C., Monteiro L.V.S., Xavier R.P., Santiago E.B.S. 2014. Geocronologia U-Pb e uma nova perspectiva sobre a evolução do depósito IOCG de classe mundial Salobo, Província Carajás, Brasil. In: Congresso Brasileiro de Geologia, 47., Salvador. *Actas...* CD-ROM.
- Mitchell J.N., Scoates J.S., Frost C.D., Kolker A. 1996. The geochemical evolution of anorthositic residual magmas in the Laramie anorthosite complex, Wyoming. *Journal of Petrology*, **37**(3):637-660. <https://doi.org/10.1093/ptro/37.3.637>
- Molin G., Zanazzi P.F. 1991. Intracrystalline Fe²⁺-Mg ordering in augite: Experimental study and geothermometric applications. *European Journal of Mineralogy*, **3**(5):863-875. <https://doi.org/10.1127/ejm/3/5/0863>
- Moreto C.P.N., Monteiro L.V.S., Xavier R.P., Amaral W.S., Santos T.J.S., Juliano C., Souza Filho C.R. 2011. Mesoarchean (3.0 and 2.86 Ga) host rocks of the iron oxide-Cu-Au Bacaba deposit, Carajás Mineral Province: U-Pb geochronology and metallogenetic implications. *Mineralium Deposita*, **46**:789-811. <https://doi.org/10.1007/s00126-011-0352-9>
- Morimoto N. 1988. Nomenclature of pyroxenes. *Mineralogy and Petrology*, **39**:55-76.
- Mutch E.J.F., Blundy J.D., Tattitch B.C., Cooper F.J., Brooker R.A. 2016. An experimental study of amphibole stability in low-pressure granitic magmas and a revised Al-in-hornblende geobarometer. *Contributions to Mineralogy and Petrology*, **171**:85. <https://doi.org/10.1007/s00410-016-1298-9>
- Nachit H., Ibhi A., Abia E.H., Ohoud M.B. 2005. Discrimination between primary magmatic biotites, reequilibrated biotites and neofomed biotites. *Comptes Rendus Geoscience*, **337**(16):1415-1420. <https://doi.org/10.1016/j.crte.2005.09.002>
- Naney M.T. 1983. Phase equilibria of rock-forming ferromagnesian silicates in granitic systems. *American Journal of Science*, **283**(10):993-1033. <https://doi.org/10.2475/ajs.283.10.993>
- Newton R.C. 1992. An overview of charnockites. *Precambrian Research*, **55**(1-4):399-405. [https://doi.org/10.1016/0301-9268\(92\)90036-N](https://doi.org/10.1016/0301-9268(92)90036-N)
- Nogueira A.C.R., Truckenbrodt W., Pinheiro R.V.L. 1995. Formação Águas Claras, Pré-Cambriano da Serra dos Carajás: Redescoberta e redefinição litoestratigráfica. *Boletim do Museu Paraense Emílio Goeldi*, **7**:177-277.
- Oliveira M.A., Dall'Agnol R., Althoff F.J., Leite A.A.S. 2009. Mesoarchean sanukitoid rocks of the Rio Maria Granite-Greenstone Terrane, Amazonian Craton, Brazil. *Journal of South American Earth Sciences*, **27**(2-3):146-160. <https://doi.org/10.1016/j.jsames.2008.07.003>
- Oliveira M.A., Dall'Agnol R., Scaillet B. 2010. Petrological constraints on crystallization conditions of Mesoarchean Sanukitoid Rocks, southeastern Amazonian craton, Brazil. *Journal of Petrology*, **51**(10):2121-2148. <https://doi.org/10.1093/ptrology/egq051>
- Oliveira V.E.S., Oliveira D.C., Marangoanha B., Lamarão C.N. 2018. Geology, mineralogy and petrological affinities of the Neoproterozoic granitoids from the central portion of the Canaã dos Carajás domain, Amazonian craton, Brazil. *Journal of South American Earth Sciences*, **85**:135-159. <https://doi.org/10.1016/j.jsames.2018.04.022>
- Percival J.A., Mortensen J.K. 2002. Water-deficient calc-alkaline plutonic rocks of northeastern Superior Province, Canada: Significance of charnockitic magmatism. *Journal of Petrology*, **43**(9):1617-1650. <https://doi.org/10.1093/ptrology/43.9.1617>
- Pichamuthu C.S. 1969. Nomenclature of charnockites. *Indian Mineralogist*, **20**(6):23-55.
- Pidgeon R., Macambira M.J.B., Lafon J.M. 2000. Th-U-Pb isotopic systems and internal structures of complex zircons from an enderbite from the Pium Complex, Carajás Province, Brazil: Evidence for the ages of granulite facies metamorphism and the source of the enderbite. *Chemical Geology*, **166**(1-2):159-171. [https://doi.org/10.1016/S0009-2541\(99\)00190-4](https://doi.org/10.1016/S0009-2541(99)00190-4)
- Prouteau G., Scaillet B. 2003. Experimental constraints on the origin of the 1991 Pinatubo dacite. *Journal of Petrology*, **44**(12):2203-2241. <https://doi.org/10.1093/ptrology/egg075>
- Putirka K.D. 2008. Thermometers and barometers for volcanic systems. Minerals, Inclusions and Volcanic Processes. *Reviews in Mineralogy & Geochemistry*, **69**(1):61-120. <https://doi.org/10.2138/rmg.2008.69.3>
- Putirka K.D. 2016. Amphibole thermometers and barometers for igneous systems and some implications for eruption mechanisms of felsic magmas at arc volcanoes. *American Mineralogist*, **101**(4):841-858. <https://doi.org/10.2138/am-2016-5506>
- Rajesh H.M. 2007. The petrogenetic characterization of intermediate and silicic charnockites in high-grade terrains: A case study from southern India. *Contributions to Mineralogy and Petrology*, **154**:591-606. <https://doi.org/10.1007/s00410-007-0211-y>
- Rajesh H.M., Santosh M. 2004. Charnockitic magmatism in southern India. Proceedings of the Indian Academy of Sciences. *Earth and Planetary Sciences*, **113**:565-585. <https://doi.org/10.1007/BF02704023>
- Rajesh H.M., Santosh M. 2012. Charnockites and charnockites. *Geoscience Frontiers*, **3**(6):737-744. <https://doi.org/10.1016/j.gsf.2012.07.001>
- Rajesh H.M., Santosh M., Yoshikura S. 2011. The Nagercoil charnockite: A magnesian, calcic to calc-alkalic granitoid dehydrated during a granulite-facies metamorphic event. *Journal of Petrology*, **52**(2):375-400. <https://doi.org/10.1093/ptrology/egq084>
- Rapopo M. 2011. *Petrogenesis of the syntectonic Matok pluton in the Limpopo belt (South Africa) and its implications on the geodynamic environment*. MS Dissertation, Faculty of Science, University of Stellenbosch, Stellenbosch (South Africa), 120 p.

- Rayleigh J.W.S. 1896. Theoretical considerations respecting the separation of gases by diffusion and similar processes. *Philosophical Magazine*, **42**(259):493-498. <https://doi.org/10.1080/14786449608620944>
- Ridley J. 1992. On the origins and tectonic significance of the charnockite suite of the Archaean Limpopo belt, northern marginal zone, Zimbabwe. *Precambrian Research*, **55**(1-4):407-427. [https://doi.org/10.1016/0301-9268\(92\)90037-0](https://doi.org/10.1016/0301-9268(92)90037-0)
- Ridolfi F., Renzulli A., Puerini M. 2010. Stability and chemical equilibrium of amphibole in calc-alkaline magmas: An overview, new thermobarometric formulations and application to subduction-related volcanoes. *Contributions to Mineralogy and Petrology*, **160**:45-66. <https://doi.org/10.1007/s00410-009-0465-7>
- Rodrigues D.S., Oliveira D.C., Macambira M.J.B. 2014. Geologia, geoquímica e geocronologia do Granito Mesoarqueano Boa Sorte, município de Água Azul do Norte, Pará – Província Carajás. *Boletim do Museu Paraense Emílio Goeldi. Série Ciências da Terra*, **9**(3):597-633. <https://doi.org/10.46357/bcnaturais.v9i3.513>
- Roeder P.L., Emslie R.F. 1970. Olivine-liquid equilibrium. *Contribution to Mineralogy and Petrology*, **29**:275-289. <https://doi.org/10.1007/BF00371276>
- Rollinson H. 1993. *Using geochemical data*. London: Longman, 384 p.
- Santos R.D., Galarza M.A., Oliveira D.C. 2013. Geologia, geoquímica e geocronologia do Diopsídio-Norito Pium, Província Carajás. *Boletim do Museu Paraense Emílio Goeldi, Série Ciências da Terra*, **8**(3):355-382. <https://doi.org/10.46357/bcnaturais.v8i3.554>
- Santosh M., Yoshikura S. 2001. Charnockite magmatism and charnockitic metasomatism in east Gondwana and Asia. *Gondwana Research*, **4**(4):768-771. [https://doi.org/10.1016/S1342-937X\(05\)70555-4](https://doi.org/10.1016/S1342-937X(05)70555-4)
- Schmidt M.W. 1992. Amphibole composition in tonalite as a function of pressure: An experimental calibration of the Al-in-hornblende barometer. *Contributions to Mineralogy and Petrology*, **110**:304-310. <https://doi.org/10.1007/BF00310745>
- Scoates J.S., Lindsley D.H. 2000. New insights from experiments on the origin of anorthosite. *EOS, Transactions of the American Geophysical Union*, **81**:1300.
- Silva F.F., Oliveira D.C., Dall'Agnol R., Silva L.R., Cunha I.V. 2020. Lithological and structural controls on the emplacement of a Neoproterozoic plutonic complex in the Carajás province, southeastern Amazonian craton (Brazil). *Journal of South American Earth Sciences*, **102**:102696. <https://doi.org/10.1016/j.jsames.2020.102696>
- Silva M.A.D., Monteiro L.V.S., Santos T.J.S., Moreto C.P.N., Sousa S.D., Faustinoni J.M., Melo G.H.C., Xavier R.P., Toledo B.A.M. 2021. Mesoarchean migmatites of the Carajás Province: From intra-arc melting to collision. *Lithos*, **388-389**:106078. <https://doi.org/10.1016/j.lithos.2021.106078>
- Souza D.B., Oliveira D.C., Monteiro L.V.S., Gabriel E.O., Marangoanha B. 2017. Colocação, metamorfismo e natureza dos anfíbolitos de Água Azul do Norte, Província Carajás. *Geologia USP. Série Científica*, **17**(4):99-123. <https://doi.org/10.11606/issn.2316-9095.v17-441>
- Souza Z.S., Potrel H., Lafon J.M., Althoff F.J., Pimentel M.M., Dall'Agnol R., Oliveira C.G. 2001. Nd, Pb and Sr isotopes of the Identidade Belt, an Archaean greenstone belt of the Rio Maria region (Carajás Province, Brazil): implications for the Archaean geodynamic evolution of the Amazonian Craton. *Precambrian Research*, **109**(3-4):293-315. [https://doi.org/10.1016/S0301-9268\(01\)00164-4](https://doi.org/10.1016/S0301-9268(01)00164-4)
- Streckeisen A. 1974. Classification and nomenclature of plutonic rocks: Recommendations of the IUGS subcommission on the systematics of igneous rocks. *Geologische Rundschau*, **63**(2):773-786. <https://doi.org/10.1007/BF01820841>
- Tassinari C.C.G., Macambira M. 2004. A evolução tectônica do Craton Amazônico. In: Mantesso-Neto V., Bartorelli A., Carneiro C.D.R., Brito Neves B.B. (eds.). *Geologia do continente sul-americano: evolução da obra de Fernando Flávio Marques Almeida*. São Paulo: Beca, p. 471-486.
- Teixeira L.R. 2005. *GENESIS 4.0 – Software de Modelamento Geoquímico*.
- Teixeira M.F.B., Dall'Agnol R., Santos J.O.S., Kemp A., Evans N. 2019. Petrogenesis of the Paleoproterozoic (Orosirian) A-type granites of Carajás Province, Amazon Craton, Brazil: Combined in situ Hf-O isotopes of zircon. *Lithos*, **332-333**:1-22. <https://doi.org/10.1016/j.lithos.2019.01.024>
- Vander Auwera J., Longhi J., Duchesne J.C. 1998. A liquid line of descent of the jotunite (hypersthene monzodiorite) suite. *Journal of Petrology*, **39**(3):439-468. <https://doi.org/10.1093/ptro/39.3.439>
- Vasquez L.V., Rosa-Costa L.R., Silva C.G., Ricci P.F., Barbosa J.O., Klein E.L., Lopes E.S., Macambira E.B., Chaves C.L., Carvalho J.M., Oliveira J.G., Anjos G.C., Silva H.R. 2008. Escala 1:1.000.000. In: Vasquez M.L., Rosa-Costa L.T. (eds.). *Geologia e recursos minerais do estado do Pará: Sistema de Informações Geográficas e SIG: texto explicativo dos mapas Geológico e Tectônico e de Recursos Minerais do Estado do Pará*. Belém: CPRM, 328 p.
- Watson E.B., Harrison T.M. 1983. Zircon saturation revisited: Temperature and composition effects in a variety of crustal magma types. *Earth and Planetary Science Letters*, **64**(2):295-304. [https://doi.org/10.1016/0012-821X\(83\)90211-X](https://doi.org/10.1016/0012-821X(83)90211-X)
- Weiss S., Troll G. 1989. The Ballachulish Igneous Complex, Scotland: Petrography, mineral chemistry and order of crystallization in the monzodiorite-quartz diorite suite and in the granite. *Journal of Petrology*, **30**(5):1069-1115. <https://doi.org/10.1093/ptrology/30.5.1069>
- Wilmart E., Clocchiatti R., Duchesne J.C., Touret L.R. 1991. Fluid inclusions in charnockites from the Bjerkreim-Sokndal massif (Rogaland, southwestern Norway): Fluid origin and in situ evolution. *Contributions to Mineralogy and Petrology*, **108**:453-462. <https://doi.org/10.1007/BF00303449>
- Wones D.R., Eugster H.P. 1965. Stability of biotite: experiment, theory, and applications. *American Mineralogist*, **50**(9):1228-1272.
- Wyers G.P., Barton M. 1986. Petrology and evolution of transitional alkaline-subalkaline lavas from Patmos, Dodecanesos, Greece: Evidence for fractional crystallization, magma mixing, and assimilation. *Contributions to Mineralogy and Petrology*, **93**:297-311. <https://doi.org/10.1007/BF00389389>
- Yang Q.Y., Santosh M. 2015. Charnockite magmatism during a transitional phase: Implications for late Paleoproterozoic ridge subduction in the North China Craton. *Precambrian Research*, **261**:188-216. <https://doi.org/10.1016/j.precamres.2015.01.014>
- Yavuz F. 2003. Evaluating micas in petrologic and metallogenic aspect: I-definitions and structure of the computer program MICA*. *Computers & Geosciences*, **29**(10):1203-1213. [https://doi.org/10.1016/S0098-3004\(03\)00142-0](https://doi.org/10.1016/S0098-3004(03)00142-0)
- Yavuz F. 2013. WinPyrox: A Windows program for pyroxene calculation classification and thermobarometry. *American Mineralogist*, **98**(7):1338-1359. <https://doi.org/10.2138/am.2013.4292>
- Yavuz F., Döner Z. 2017. WinAmptb: A Windows program for calcic amphibole thermobarometry. *Periodico di Mineralogia*, **86**(2):135-167. <https://doi.org/10.2451/2017PM710>
- Young D.N., Zhao J.X., Ellis D.J., McCulloch M.T. 1997. Geochemical and Sr-Nd isotopic mapping of source provinces for the Mawson charnockites, east Antarctica: Implications for Proterozoic tectonics and Gondwana reconstruction. *Precambrian Research*, **86**(1-2):1-19. [https://doi.org/10.1016/S0301-9268\(97\)00030-2](https://doi.org/10.1016/S0301-9268(97)00030-2)
- Zhao K., Xu X., Erdmann S. 2018. Thermodynamic modeling for an incrementally fractionated granite magma system: Implications for the origin of igneous charnockite. *Earth and Planetary Science Letters*, **499**:230-242. <https://doi.org/10.1016/j.epsl.2018.07.039>